2011

# Reduced Utilization of Selenium by Naked Mole Rats Due to a Specific Defect in GPx1 Expression

Marina V. Kasaikina
*University of Nebraska-Lincoln*, kasaikina@yahoo.com

Alexei V. Lobanov
*Brigham and Women's Hospital and Harvard Medical School*

Mikalai I. Malinouski
*University of Nebraska - Lincoln*, mmalinouski2@unl.edu

Byung Cheon Lee
*Brigham and Women's Hospital and Harvard Medical School*, cheonii@yahoo.com

Javier Seravalli
*University of Nebraska-Lincoln*, jseravalli1@unl.edu

*See next page for additional authors*

THE JOURNAL OF BIOLOGICAL CHEMISTRY VOL. 286, NO. 19, pp. 17005–17014, May 13, 2011
Printed in the U.S.A.



# Reduced Utilization of Selenium by Naked Mole Rats Due to a Specific Defect in GPx1 Expression*[S]

Received for publication, December 27, 2010, and in revised form, March 3, 2011 Published, JBC Papers in Press, March 3, 2011, DOI 10.1074/jbc.M110.216267

**Marina V. Kasaikina[‡§], Alexei V. Lobanov[‡], Mikalai Y. Malinouski[‡§], Byung Cheon Lee[‡§], Javier Seravalli[§], Dmitri E. Fomenko[§], Anton A. Turanov[‡], Lydia Finney[¶], Stefan Vogt[‖], Thomas J. Park[**], Richard A. Miller[‡‡], Dolph L. Hatfield[§§], and Vadim N. Gladyshev[‡§1]**

*From the [‡]Division of Genetics, Department of Medicine, Brigham and Women's Hospital and Harvard Medical School, Boston, Massachusetts 02115, the [§]Department of Biochemistry and Redox Biology Center, University of Nebraska, Lincoln, Nebraska 68588, the [¶]Biosciences Division and [‖]X-ray Science Division, Argonne National Laboratory, Argonne, Illinois 60439, the [**]Department of Biological Sciences, University of Illinois, Chicago, Illinois 60607, the [‡‡]University of Michigan, Ann Arbor, Michigan 48109, and the [§§]Molecular Biology of Selenium Section, Laboratory of Cancer Prevention, Center for Cancer Research, NCI, National Institutes of Health, Bethesda, Maryland 20892*

**Naked mole rat (MR) *Heterocephalus glaber* is a rodent model of delayed aging because of its unusually long life span (>28 years). It is also not known to develop cancer. In the current work, tissue imaging by x-ray fluorescence microscopy and direct analyses of trace elements revealed low levels of selenium in the MR liver and kidney, whereas MR and mouse brains had similar selenium levels. This effect was not explained by uniform selenium deficiency because methionine sulfoxide reductase activities were similar in mice and MR. However, glutathione peroxidase activity was an order of magnitude lower in MR liver and kidney than in mouse tissues. In addition, metabolic labeling of MR cells with $^{75}$Se revealed a loss of the abundant glutathione peroxidase 1 (GPx1) band, whereas other selenoproteins were preserved. To characterize the MR selenoproteome, we sequenced its liver transcriptome. Gene reconstruction revealed standard selenoprotein sequences except for GPx1, which had an early stop codon, and SelP, which had low selenocysteine content. When expressed in HEK 293 cells, MR GPx1 was present in low levels, and its expression could be rescued neither by removing the early stop codon nor by replacing its SECIS element. In addition, GPx1 mRNA was present in lower levels in MR liver than in mouse liver. To determine if GPx1 deficiency could account for the reduced selenium content, we analyzed GPx1 knock-out mice and found reduced selenium levels in their livers and kidneys. Thus, MR is characterized by the reduced utilization of selenium due to a specific defect in GPx1 expression.**

Naked mole rat (MR)[2] (*Heterocephalus glaber*) is a unique organism in the mammalian order rodentia. It is an attractive model to study aging due to an extraordinary life span (more than 28 years), which is unprecedented for rodents of similar body size. Aging in MRs is characterized by very slow age-related declines that do not significantly affect breeding capacity, social behavior, and daily activity (1–3). MR evolved a unique eusocial lifestyle with strictly determined social roles and cooperative breeding within the colony. The anatomy of MR has several specific features, which probably evolved as an adaptation to living underground in oxygen-limiting conditions, including underdevelopment of the visual system (4), skin insensitivity (5), and the ability to tolerate low temperature (6) and low oxygen levels (7). MRs are also characterized by a decreased metabolic rate, which is associated with reduced levels of thyroid hormones (3). One of the most remarkable features of MR is that none of the autopsies of dead animals in several colonies revealed cancer incidence (1). Moreover, primary fibroblasts derived from MR were sensitive to contact inhibition (8), resistant to experimentally induced tumorigenesis, and unable to form xenograft tumors (9).

MR poses a challenge to the theories that link aging, cancer, and oxidative stress. Because MR lives in low oxygen conditions, it is expected to have low levels of oxidative stress. However, research showed that MR is characterized by significant oxidative damage. Compared with mice, MRs have a lower GSH/GSSG ratio, higher rate of lipid peroxidation, higher rate of DNA oxidative damage, and higher protein carbonylation (10). It was also demonstrated that MR proteins possess higher levels of protein thiols, increased protein stability, increased resistance to urea-induced denaturation, and elevated proteasomal activity while also showing lower levels of protein ubiquitination. Moreover, unlike the mouse proteome, the MR proteome did not show significant age-related susceptibility to oxidation and ubiquitination (11). A separate study did not detect age-related changes in the activities of antioxidant enzymes, including Mn-superoxide dismutase, Cu/Zn-super-

* This work was supported, in whole or in part, by National Institutes of Health Grants GM061603, CA080946, and AG021518 (to V. N. G.) and the Intramural Research Program of the Center for Cancer Research, NCI, National Institutes of Health (to D. L. H.). This work was also supported by the Department of Energy Office of Science under Contract DE-AC02-06CH11357.

[S] The on-line version of this article (available at http://www.jbc.org) contains supplemental Figs. S1–S18.

[1] To whom correspondence should be addressed: Division of Genetics, Department of Medicine, Brigham and Women's Hospital and Harvard Medical School, New Research Bldg., Rm. 435, 77 Ave. Louis Pasteur, Boston, MA 02115. Tel.: 617-525-5122; E-mail: vgladyshev@rics.bwh.harvard.edu.

[2] The abbreviations used are: MR, naked mole rat (*H. glaber*); ICP-MS, inductively coupled plasma mass spectrometry; GPx, glutathione peroxidase; MsrA, methionine-*S*-sulfoxide reductase; MsrB, methionine-*R*-sulfoxide reductase; Sec, selenocysteine; SECIS, selenocysteine insertion sequence; SelP, selenoprotein P; XFM, x-ray fluorescence microscopy; contig, group of overlapping clones; EGFP, enhanced green fluorescent protein; BisTris, 2-[bis(2-hydroxyethyl)amino]-2-(hydroxymethyl)propane-1,3-diol.

oxide dismutase, and catalase, and also observed low glutathione peroxidase (GPx) activity (12).

Mammals have eight GPxs, including five selenoproteins. GPx1 is the first identified and one of the best studied selenoproteins (13). This and other selenoprotein GPxs have selenocysteine (Sec) residues in their active sites. GPx1 is a cytosolic enzyme and the most abundant selenoprotein in mammals. Other GPxs show different cellular localizations and/or tissue and substrate specificities (14, 15). GPx1 is not an essential enzyme (*i.e.* GPx1 knock-out mice are viable and fertile). However, GPx1 knock-out mice are more susceptible to oxidative stress (16, 17) and viral myocardites (18). Expression of GPx1 is decreased in prostate cancer and breast cancer cell lines (19) as well as in the mouse model of liver cancer (20). A single nucleotide polymorphism that changes Pro to Leu at codon 198 of human GPx1 is associated with lung (21) and bladder (22) cancers.

Currently, there is no information on the utilization of selenium by MR; however, this is an essential trace element in mammals, and its supplementation may be beneficial in cancer chemoprevention (23). Selenium functions mostly through incorporation into proteins in the form of Sec. Mice and humans have 24 and 25 selenoprotein genes, respectively (24). However, nothing is known about the composition of the MR selenoproteome.

In this study, we observed low levels of selenium in MR tissues. This observation led to the finding that the reduced utilization of selenium by this organism was due to a specific defect in GPx1 expression.

## EXPERIMENTAL PROCEDURES

*Animals*—Animal experiments were approved by institutional animal care and use committees at the University of Illinois (Chicago, IL) and University of Nebraska (Lincoln, NE). To carry out inductively coupled plasma mass spectrometry (ICP-MS) analyses, Western blotting, activity assays, and other analyses, animals were sacrificed, and their tissues were frozen in liquid nitrogen and stored until use. To prepare extracts, tissues were homogenized in PBS supplemented with a protease inhibitor mixture (Sigma). Cellular debris was removed by centrifugation at 13,000 rpm for 15 min at 4 °C, and protein concentrations were determined by the Bradford assay.

*Tissue Samples for X-ray Fluorescence Microscopy (XFM)*—Tissues from C57BL/6 mice and MRs were extracted and prepared at the same time to match preparation conditions. Mice were fed a standard rodent chow diet. MRs were fed either a sweet potato or carrot diet. Tissues from a 1-year-old MR were compared with the corresponding samples of a 2-month-old mouse to adjust for life span differences. All freshly extracted tissues were washed in PBS and placed in 4% neutral buffered formaldehyde in PBS for fixation. After 12 h, tissues were transferred to PBS, paraffin-embedded, and cut using a standard microtome into 5-$\mu$m sections. Sections were mounted on silicon nitride windows (2 × 2 mm, 200-nm thickness; Silson, Blisworth, UK). Light microscopy images were taken using a Leica DMXR microscope (Leica Microsystems, Bannockburn, IL).

*XFM*—Trace elements in mouse and MR tissue samples were imaged with XFM at the Advanced Photon Source, Argonne National Laboratory (Argonne, IL). For each pixel, the full x-ray fluorescence spectrum was recorded using a single-element silicon drift detector (Vortex EX, SII Nanotechnology, Northridge, CA). Dwell time varied from 1.1 to 4 s/pixel. For quantification, each set of experiments was followed by recording x-ray fluorescence spectra of thin film standards NBS-1832 and NBS-1833 (National Bureau of Standards). X-ray fluorescence spectra for each sample were fitted and quantified using data derived from standards. Image processing and analysis were performed using MAPS software (25). Each x-ray fluorescence image represents two-dimensional distribution of the element.

*Activity Assays*—Total GPx activity was measured using a GPx activity kit (Sigma) according to the manufacturer's instructions. Methionine-*S*-sulfoxide reductase (MsrA) and methionine-*R*-sulfoxide (MsrB) activities were measured in an HPLC assay as described (26). Briefly, 200 $\mu$g of total protein were added to a reaction mixture that was kept at 37 °C for 30 min in the presence of 20 mM DTT and either 200 $\mu$M dabsyl-methionine-*S*-sulfoxide (to assay for MsrA activity) or 200 $\mu$M dabsyl-methionine-*R*-sulfoxide (to assay for MsrB activity). After stopping the reaction by adding 200 $\mu$l of acetonitrile, it was centrifuged at 4 °C for 15 min at 13,000 rpm, and the supernatant (50 $\mu$l) was injected onto a $C_{18}$ column (ZORBAX Eclipse XDB-C18) to quantify the resulting dabsylated methionine.

*Splenocyte Isolation and $^{75}$Se Metabolic Labeling*—After dissection, spleen was immediately transferred into ice-cold DMEM and mashed through a 45-$\mu$m cell strainer into the 50-ml tube. Cells were centrifuged at 800 × *g* for 5 min. The pellet was resuspended in 5 ml of ASK buffer (Invitrogen) and incubated at room temperature for 5 min. Cells were then diluted with DMEM and pelleted at 800 rpm for 5 min. The resulting pellet was resuspended in 15 ml of DMEM supplemented with 10% fetal bovine serum (Invitrogen), antibiotic/antimicotic (Invitrogen), 0.4 mM glutamine, and freshly neutralized $^{75}$Se selenious acid (specific activity 1000 Ci/mmol, final concentration in the medium 1 nM) and pooled into a 15-cm plate. After 24 h, cells were washed three times with ice-cold PBS and lysed in CellLytic buffer (Sigma). Protein extracts were analyzed by SDS-PAGE followed by autoradiography.

*Whole Transcriptome Sequencing and Assembly of Selenoprotein Genes*—Extraction of the total RNA from MR liver was carried out using an RNAqueous kit (Ambion) according to the manufacturer's instructions. DNA was removed by treatment with DNase I (Ambion). Liver transcriptome was sequenced at the University of Nebraska-Lincoln genomic facility on an Illumina instrument. To assemble 35-bp reads into longer contigs, three different strategies were used. First, mapping of reads to reference sequence from mouse or guinea pig genomes was performed using the MAQ package 0.7.1 (available from the Sourceforge Web site). Second, SOAP package 1.03 (available from the Short Oligonucleotide Analysis Package Web site) was used for *de novo* assembly of short reads. Finally, we employed an in-house program that was optimized for assembling selenoprotein genes and utilized the variety of information available

from MAQ and SOAP output as well as known sequences from other rodents.

*ICP-MS*—Quantitative analyses of trace elements in animal tissues were performed using ICP-MS. Freshly frozen mouse and MR tissues were homogenized and sonicated in PBS with Complete protease inhibitor mixture (Roche Applied Science) (1 tablet in 50 ml of PBS). Samples were normalized to protein content in each lysate, as determined using the Bradford Protein Kit (Bio-Rad). Samples were digested in 15% nitric acid, 15% hydrogen peroxide for 2 h at 70 °C. 50 ppb gallium were added as an internal control to the digestion mix. After digestion, samples were diluted 10 times with deionized water and analyzed by ICP-MS. Elemental analysis was performed at the University of Nebraska-Lincoln Spectroscopy Core Facility using an Agilent Technologies ICP-MS model 7500ce (Santa Clara, CA) and an Elemental Scientific Inc. (Omaha, NE) SC4 autosampler. Each sample was analyzed in triplicate. The carrier and make-up gas flows were 0.95 and 0.15 liter/min of argon, respectively. The collision cell operated with 3.5 ml/min $H_2$ and 1.5 ml/min helium for reaction/collision mode. Dwell times for all elements were 0.3 s except $^{78}$Se, for which the dwell time was set at 0.9 s. Gallium ($m/z = 71$) was added to all samples and standards as an internal standard at 50 ppb.

*Expression Constructs for Mouse and MR GPx1 and Their Mutants*—Mouse and MR GPx1 cDNAs containing the 3′-UTRs, including SECIS elements, were amplified by a two-step PCR with primers that introduced Myc tag into ORFs. Primers were designed as follows: mouse first round (CTCAGAGGAGGATCTCTGTGCTGCTCGGCTCTCCG and GCATACTCTAGACTGATATTCAGCACTTTATTCTTAGTAGTGAAACC) and second round (CTCAGAGGAGGATCTCTGTGCTGGTCGTTTGGCCGCGGCC and GCATACTCTAGACTGATATTCAGCACTTTATTCTTAGTAGTGAAACC); MR first round (CTCAGAGGAGGATCTCTGTGCTGGTCGTTTGGCCGCGGCC and GCATACTCTAGAACACCCAGCACTTTATTAGAGGGTAATCATTTTGG) and second round (GCATACTCTAGAACACCCAGCACTTTATTAGAGGGTAATCATTTTGG and ATGACATCTCGAGATGGAGCAGAAGCTCATCTCAGAGGAGGATCTC). The PCR products were digested with XhoI and Xba and ligated into a similarly digested pCIneo vector. In the case of mouse GPx1, an early premature stop codon was introduced using site-directed mutagenesis with the QuikChange kit (Stratagene) and primers GAAACCCTGCTGTCCTAGCAGTCTGGCAAC and GTTGCCAGACTGCTAGGACAGCAGGGTTTC. The resulting mutant was designated as the M-short form. To rescue the early stop codon in MR GPx1, we performed site-directed mutagenesis with primers AAGCCCTACTCACTCAGGGGCGCGGCCCTG and CAGGGCCGCGCCCCTGAGTGAGTAGGGCTT, and the resulting mutant was designated as the MR-long form. To obtain cysteine mutants of mouse and MR GPx1, we used site-directed mutagenesis with primers TCGCGTCTCTCTGCGGCACCACGAT and ATCGTGGTGCCGCAGAGAGACGCGA for mouse GPx1 and GAATGTGGCATCCCTCTGCGGCACCACGGTC and GACCGTGGTGCCGCAGAGGGATGCCACATTC for MR GPx1. To obtain a pBudGE/GFP construct, EGFP was amplified from pEGPFN3 vector with primers ATGACAAGCTTATGGTGAGCAAGGGCGAGG and GGACATTCTAGATTACTTGTACAGCTCGTCC. The resulting PCR product was ligated into a similarly digested pBudCE4.1 vector. Mouse and MR GPx1 mutants were amplified from pCIneo constructs with primers GGTACCATGGAGCAGAAGCTCATCTCAGAGG/GCATACGCATACAGATCTCTGATATTCAGCACTTTATTCTTAG and GGTACCATGGAGCAGAAGCTCATCTCAGAGG/AGATCTACACCCAGCACTTTATTAGAGG, respectively, and inserted into the second multiple cloning site of the pBudCE4.1/GFP vector at Bglll/Kpnl restriction sites. Cys mutants were amplified with GGTACCATGGAGCAGAAGCTCATCTCAGAGG and GCATACAGATCTTTAGGAGTTGCCAGACTGC (mouse) and GGTACCATGGAGCAGAAGCTCATCTCAGAGG and GCATACAGATCTCTATGCAGGGCCGCGCCCC (MR) and inserted into the vector without the 3′-UTR. To express mouse and MR GPx1 mutants in a bacterial expression system, GPx1 mutants were amplified with primers ATGCATCATATGGAGCAGAAGCTCATCTCAGAGG and GCATGCTCGAGTTAGGAGTTGCCAGACTGC (mouse) and ATGCATCATATGTGTGCTGGTCGTTTGGCCG and GCATGCTCGAGCTATGCAGGGCCGCGCCCC (MR) and cloned into pET28a expression vector at NdeI and XhoI sites.

To clone mouse and MR GPx1 into pSelExpress1, mouse and MR GPx1 coding sequences were amplified with ATGACATAAGCTTATGGAGCAGAAGCTCATCTCAGAGG and GCATACTCTAGATTAGGAGTTGCCAGACTGC (mouse) and ATGACATAAGCTTATGGAGCAGAAGCTCATCTCAGAGG and GCATACTCTAGACTATGCAGGGCCGCGCCCC (MR) primers, digested with HindIII and XbaI restriction endonucleases, and ligated into pSelExpress1 vector. To swap mouse and MR 3′-UTRs, we prepared the corresponding constructs on the basis of the pBudCE4.1/GFP vector, which expressed Myc-tagged GPx1 and GFP from separate sites in the construct.

*Cell Culture, Transfections, Metabolic Labeling, Immunoprecipitation, and Western Blot Analyses*—HEK 293 and HeLa cells were cultured in DMEM supplemented with 10% FBS, 100 units/ml penicillin, and 100 units/ml streptomycin. All transfections were performed with Lipofectamine transfection reagent (Invitrogen), according to the manufacturer's manual. Eighteen hours after transfection, medium was replaced with one containing freshly neutralized $^{75}$Se selenious acid (specific activity 1000 Ci/mmol, final concentration in the medium 1 nM). Cells were labeled for 24 h, and cellular extracts were analyzed by SDS-PAGE followed by autoradiography. For immunoprecipitation, HEK 293 cells were grown on 10-cm plates, transfected with various GPx1 constructs, and metabolically labeled with $^{75}$Se. Cells were resuspended in PBS, supplemented with protease inhibitor mixture (Sigma), and treated with a tissue homogenizer. 600 $\mu$g of total protein were subjected to immunoprecipitation with the Protein G immunoprecipitation kit with mouse anti-Myc antibodies (Invitrogen), according to the manufacturer's instructions. For Western blot analyses, samples were separated on 10% BisTris gels, transferred onto PVDF membranes, and incubated with mouse anti-Myc (Invitrogen) or anti-GFP (Sigma) antibodies.

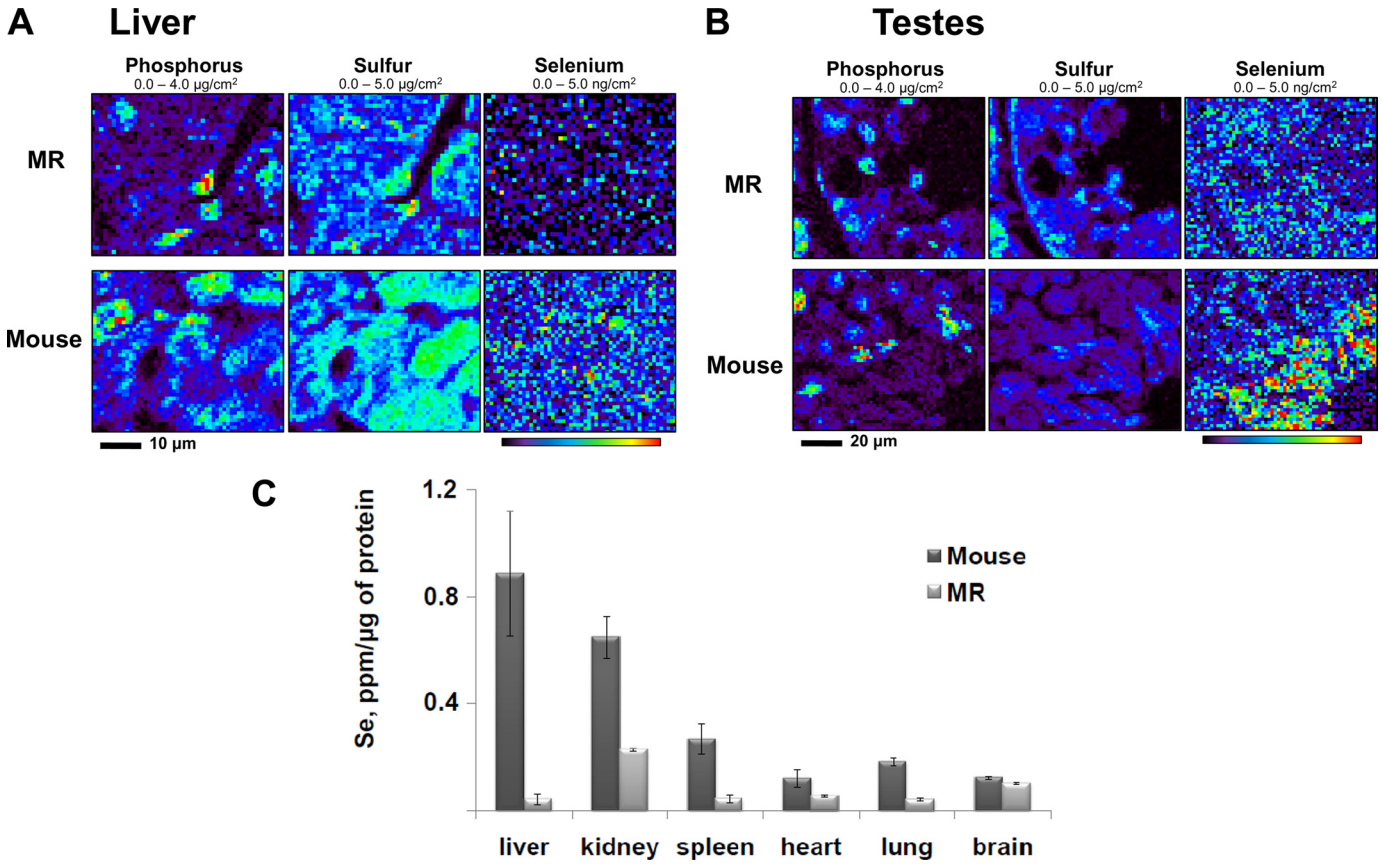


FIGURE 1. **XFM and ICP-MS analysis of selenium in mouse and MR tissues.** Shown are XFM scans of mouse and MR livers (*A*) and testes (*B*). Each element and its maximum and minimum threshold values are given *above* each *image* in ng/cm$^2$. The *rainbow-colored scale bar* relates to the signal intensity measured as ng/cm$^2$ in each spot, with *dark pixels* representing areas of low concentration and a gradient to *bright pixels* depicting increasing concentrations. A *scale bar* is shown *below* the elemental maps. *C*, selenium was analyzed by ICP-MS in mouse and MR tissues. Values are means ± S.D. (*error bars*). Organs in which trace elements were analyzed are shown *below* each *panel*.

*RNA Isolation and Quantitative PCR*—To compare GPx1 expression levels in mice and MRs, total liver RNA was isolated by TRIzol extraction according to the manufacturer's instructions. Genomic DNA was removed using a DNA removal kit (Ambion). RNA concentration was measured spectrophotometrically, and cDNA was obtained with Superscript III reverse transcriptase (Invitrogen) using the oligo(dT) primer. Real-time PCR was performed using a Fast SYBR Green master mix (Applied Biosystems). Primer sequences for the GPx1 expression analysis were as follows: mouse, CAGGAGAATGGCAAGAATGAAG and GAAGGTAAAGAGCGGGTGAG; MR, GACACCAGGAAAACGCAAAG and AAGGTGAAGAGCGGATGTG (primers were based on the assembled transcriptome sequences). GPx1 expression was normalized to that of aldolase. Primers for aldolase expression were as follows: mouse, GTGATCCTTTTCTACGAGACCC and ACCACAATTCCCTTCTCCTTG; MR, AAGATGGGTGTGACTTTGGG and GGTACTAGCCCATTCTGTTGAC.

*Additional Analyses of mRNAs*—RNA was isolated from cells transfected with various GPx1 constructs inserted into pBudCE/GFP vector. It was then treated with RNase-free DNase I (Fermentas). The resulting RNA samples were reverse transcribed with a SuperScript VILO cDNA synthesis kit (Invitrogen). Quantitative PCR was performed using a Fast SYBR Green Master Mix (Applied Biosystems). To distinguish recombinant GPx1 from the endogenous form, we used the direct primer specific for Myc-tag (TCATCTCAGAGGAGGATCTC) and reverse primers as follows: TGAGCCTTCTCACCATTCACTTCG (mouse) and CGAGCACTACCAGGCCTCTGG (MR). Expression of GPx1 mutants was normalized to EGFP expressed from the same vector. Primers for EGFP were as follows: TCAAGGACGACGGCAACTAC and TTGTGCCCCAGGATGTTGCC.

*Protein Isolation and Activity Assays*—Recombinant cysteine GPx1 mutants were expressed in BL21(DE3) cells (Novagen). *E. coli* cells were transformed with various GPx1 constructs, and the cells were grown until an OD of 0.6 at 600 nm. Protein expression was induced overnight with 1 mM isopropyl 1-thio-β-D-galactopyranoside. Cells were harvested by centrifugation, homogenized in 50 ml of PBS supplemented with Protease Inhibitor Mixture EDTA-free (Roche Applied Science), and sonicated on ice for 20 min. The suspension was centrifuged at 9000 rpm, and the resulting lysates were assayed for protein concentration and fractionated on a TALON$^{TM}$ column (Clontech). Fractions containing GPx1 mutants were dialyzed against PBS and subjected to activity assays using a GPx kit (Sigma).

## RESULTS

*Low Levels of Selenium in MR Tissues*—We analyzed the levels and distribution of selenium in various tissues of MR,

*H. glaber*. Mouse tissues were used for comparison because mice are rodents of similar size. Paraffin-embedded tissue sections were first imaged using synchrotron XFM. Selenium was uniformly distributed in liver (Fig. 1*A*), heart, and lung tissues in both organisms. Mouse testes are known to accumulate selenium in elongating spermatids (28). However, such selenium enrichment was not observed in MR testes (Fig. 1*B*). We estimated selenium content in specific areas of MR and mouse tissues (supplemental Fig. S1). Most MR tissues had considerably lower selenium levels (30–75% lower). However, MR and mouse brain samples had similar selenium contents. The brain is known to retain selenium during deficiency (29).

To verify the XFM observation of low selenium in MR tissues, we measured selenium in MR and mouse tissues using ICP-MS. All MR tissues analyzed, except the brain, had lower selenium levels than the corresponding mouse tissues (Fig. 1*C*). The major selenium pool in mice is in the liver; however, MR liver had low amounts of selenium. Thus, MR is characterized by apparent selenium deficiency.

*Low GPx Activity in MR Tissues*—Because selenium mostly occurs in the form of Sec in proteins, the low selenium in MR tissues suggested a decreased expression of selenoproteins. To test this hypothesis, we assayed methionine sulfoxide reductase and GPx activities. Mammals have three MsrBs, including the selenoprotein MsrB1, which is the major MsrB in mouse liver (30). Because it is responsible for MsrB activity in the cytosol and nucleus (MsrB2 and MsrB3 are mitochondrial and endoplasmic reticulum proteins, respectively), it is probably the main MsrB in all mammals. MsrB1 expression and activity (as well as total MsrB activity) depend on dietary selenium. Mammals also have a single MsrA, which is not a selenoprotein. We found that both MsrA and MsrB activities were similar in mice and MRs (Fig. 2, *A* and *B*). Thus, low selenium in MR tissues cannot be explained by uniform selenoprotein deficiency.

GPx1 is a major mammalian GPx, which is, like MsrB1, easily regulated by dietary selenium. We found extremely low GPx activity in MR liver compared with the corresponding mouse tissue (Fig. 2*C*). Low selenium in the liver correlated with low GPx activity, which was suggestive of low GPx1 expression.

*Sequencing and Analysis of the MR Liver Transcriptome*—Several rodent genomes were sequenced in recent years, but the genome of MR is not available. To characterize selenoprotein occurrence in MRs, we performed sequencing of the MR liver transcriptome using Illumina technology. Overall, 25,011,515 36-bp-long reads were obtained and assembled into contigs. The length distribution of assembled contigs is shown in Fig. 3*A*. The best results were obtained using k-mer size of 23, wherein 395,038 contigs were generated, with 40,073 contigs longer than 100 bp and 379 contigs exceeding 1000 bp.

Occurrence of selenoprotein genes was then examined, and we detected 15 selenoprotein sequences. This analysis suggested that the MR selenoproteome is similar to that of other mammals. Schematic representation of the human selenoproteome (which contains 25 selenoproteins) is shown in Fig. 3*B*, with MR orthologs identified in the current study highlighted. The lack of some selenoprotein genes was probably due to insufficient sequencing depth, but it also could be an indicator of their low expression in MR liver. Overall, although selenium

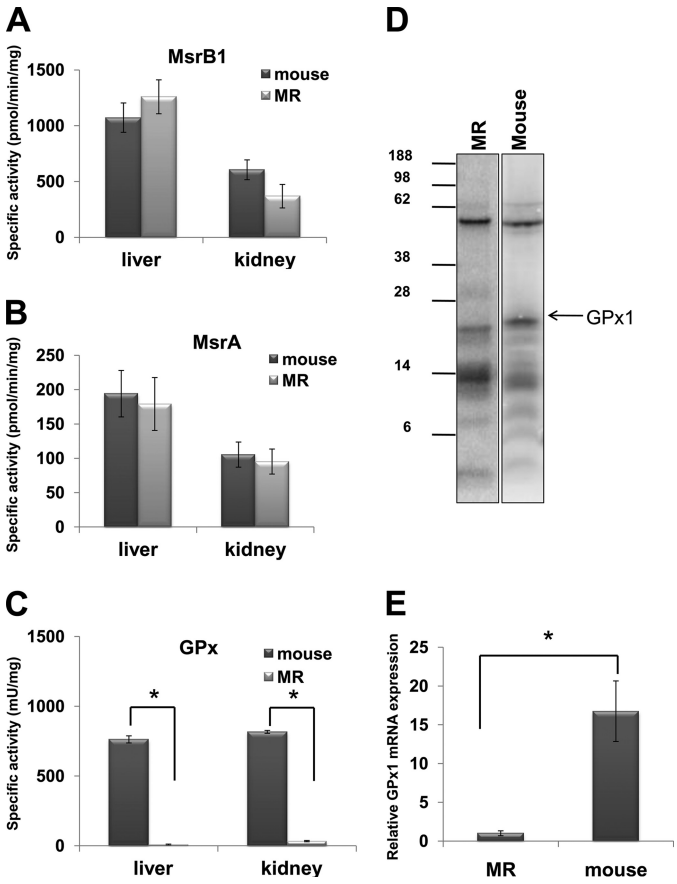


FIGURE 2. **MR tissue extracts have low GPx1 expression and activity.** Total MsrB (*A*), MsrA (*B*), and GPx (*C*) activities were measured in the indicated mouse and MR tissues. *D*, primary splenocytes derived from MR and mice were metabolically labeled with $^{75}Se$, and protein extracts were analyzed by SDS-PAGE followed by autoradiography. The band corresponding to GPx1 is shown with an *arrow* on the *right*. *E*, relative expression of GPx1 mRNA in MR and mouse liver (*, $p < 0.05$). *Error bars*, S.D.

levels and GPx activity were low in MR liver, this organ expressed many selenoprotein mRNAs, and the majority of these sequences had no unusual features (supplemental Figs. S2–S16).

SelP is the only mammalian selenoprotein that contains more than one Sec, and it has two SECIS elements in the 3′-UTR. Mammalian SelPs generally have 10–15 Sec residues (*e.g.* 10 Sec residues in human, mouse, and rat SelPs) (31). However, we found only 7 Sec residues in MR SelP (supplemental Fig. S2). Together with SelP from *Cavia porcellus*, this is the lowest Sec content of any vertebrate SelP.

In addition, we detected an unusual feature in MR GPx1: an early stop codon present five codons upstream of the position terminating GPx1 synthesis in other mammals (Fig. 3*C* and supplemental Fig. S3). Thus, MR GPx1 was predicted to be 5 amino acids shorter than other mammalian GPx1s. SECIS elements in MR selenoprotein genes satisfied the requirements of a canonical eukaryotic SECIS model. Overall, it is likely that the MR selenoproteome is not significantly different from that of other mammals, with the exception of SelP and GPx1 sequences.

*Low GPx1 Expression in MR*—To test for GPx1 expression levels, we isolated mouse and MR splenocytes and metaboli-

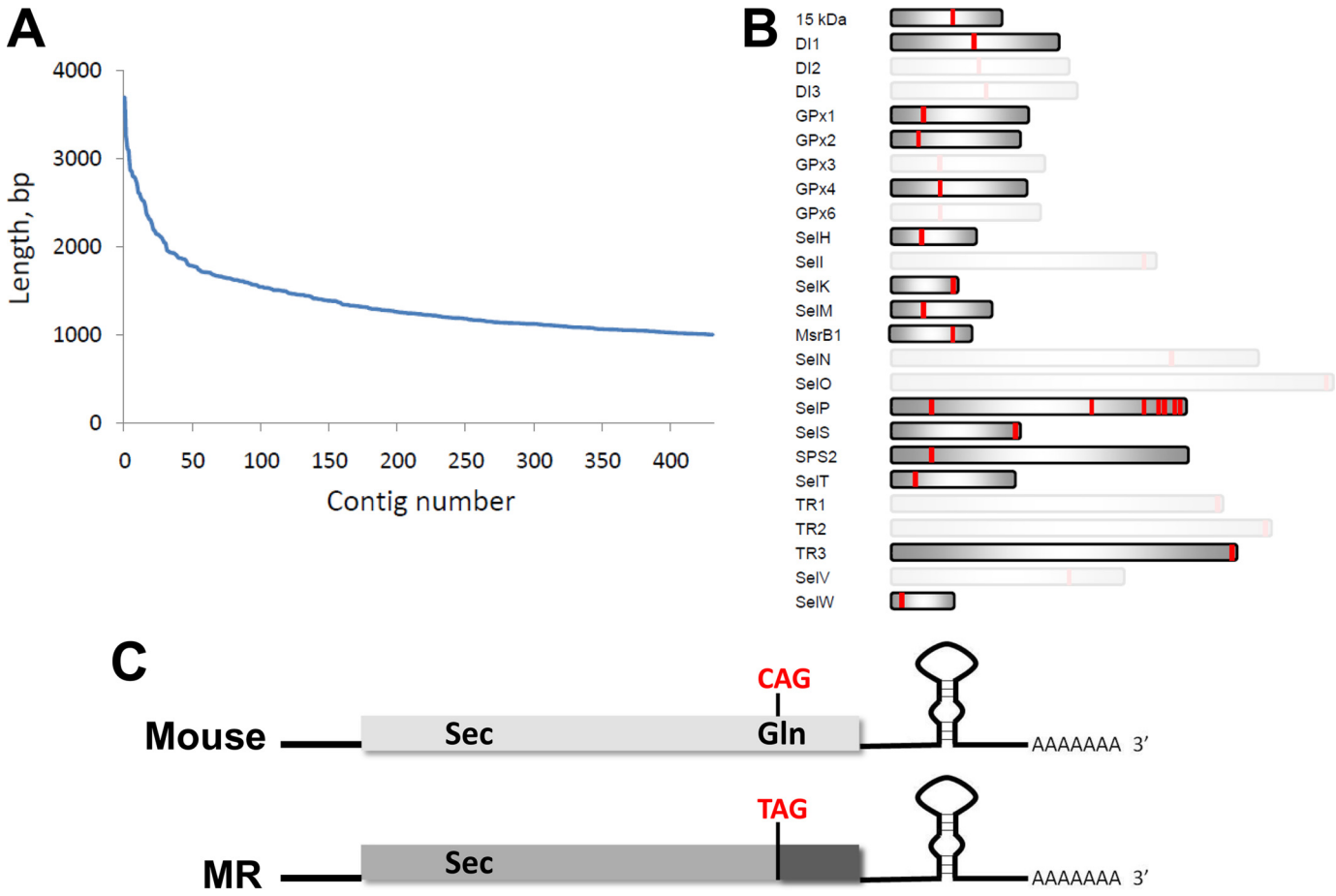


FIGURE 3. **Transcriptome analysis and characterization of the MR selenoproteome.** *A*, length distribution of assembled contigs of the MR liver transcriptome. *B*, selenoproteins identified in MR. The human selenoproteome is used as a reference to represent the MR selenoproteome. Selenoproteins identified by sequencing the MR liver transcriptome are *highlighted*. The location of Sec residues is indicated by a *red line*. Seven Sec residues were found in SelP. GPx1 has an early termination codon (see "Results"). *C*, schematic representation of MR GPx1 in comparison with mouse GPx1.

cally labeled the cells with $^{75}$Se, and they were analyzed by SDS-PAGE followed by autoradiography (Fig. 2*D*). It appeared that the GPx1 band was missing in MR splenocytes. To test if low GPx1 expression and activity were due to a low mRNA expression, GPx1 mRNA levels were examined by real-time PCR. We found that the MR GPx1 mRNA was expressed at much lower levels than mouse GPx1 mRNA in the liver (Fig. 2*E*). Thus, the low GPx1 activity was, at least in part, due to low GPx1 mRNA levels.

*Reduced Expression of MR GPx1 in Transfected Mammalian Cells*—An early stop codon in MR GPx1 could also contribute to the low expression and activity of GPx1. To test this possibility, we prepared constructs containing MR GPx1 with the early UAG stop codon and the one where UAG was replaced with CAG (encoding glutamine present in mouse GPx1 at this position). As a control, we prepared mouse GPx1 and its mutant, in which the CAG codon was changed to UAG (Fig. 4*A*). The constructs were transfected into HEK 293 cells, which were then labeled with $^{75}$Se and analyzed for selenoprotein expression patterns (Fig. 4*C*, *top*). The same membrane was also subjected to Western blot analysis with anti-Myc antibodies (Fig. 4*C*). To distinguish exogenous selenoproteins from the endogenous GPx1, proteins were immunoprecipitated with anti-Myc antibodies and analyzed on a gel (Fig. 4*C*, *bottom*). Expression levels of MR GPx1 were much lower than that of mouse GPx1. Introduction of CAG in place of UAG further decreased MR GPx1 expression. At the same time, substitution of CAG with UAG in mouse GPx1 did not decrease GPx1 expression.

In addition, mouse and MR GPx1 forms were cloned into a pBudCE4.1 vector, containing GFP under the CMV promoter. In further experiments, GFP was used as an internal control for transfection and protein loading. Inhibition of proteasome in HEK 293 cells did not rescue MR GPx1 expression (Fig. 4*D*). In addition, real time PCR analysis revealed no difference between mouse and MR GPx1 mRNA after transfection (Fig. 4*B*). Thus, MR GPx1 expression was suppressed regardless of the early stop codon. However, substitution of Sec with cysteine partially rescued expression of MR GPx1 (Fig. 4*E*). These data suggest that incorporation of Sec may limit GPx1 synthesis. We also checked if the early stop codon in MR GPx1 affects peroxidase activity of this enzyme by expressing Cys-containing His-tagged MR and mouse GPx1s in bacteria. These mouse and MR GPx1 proteins had similar activities (supplemental Fig. S17). The data suggest that the early stop codon affects neither expression nor activity of the enzyme and that the low expression of MR GPx1 is due to a combination of low mRNA levels and decreased Sec insertion. These two factors

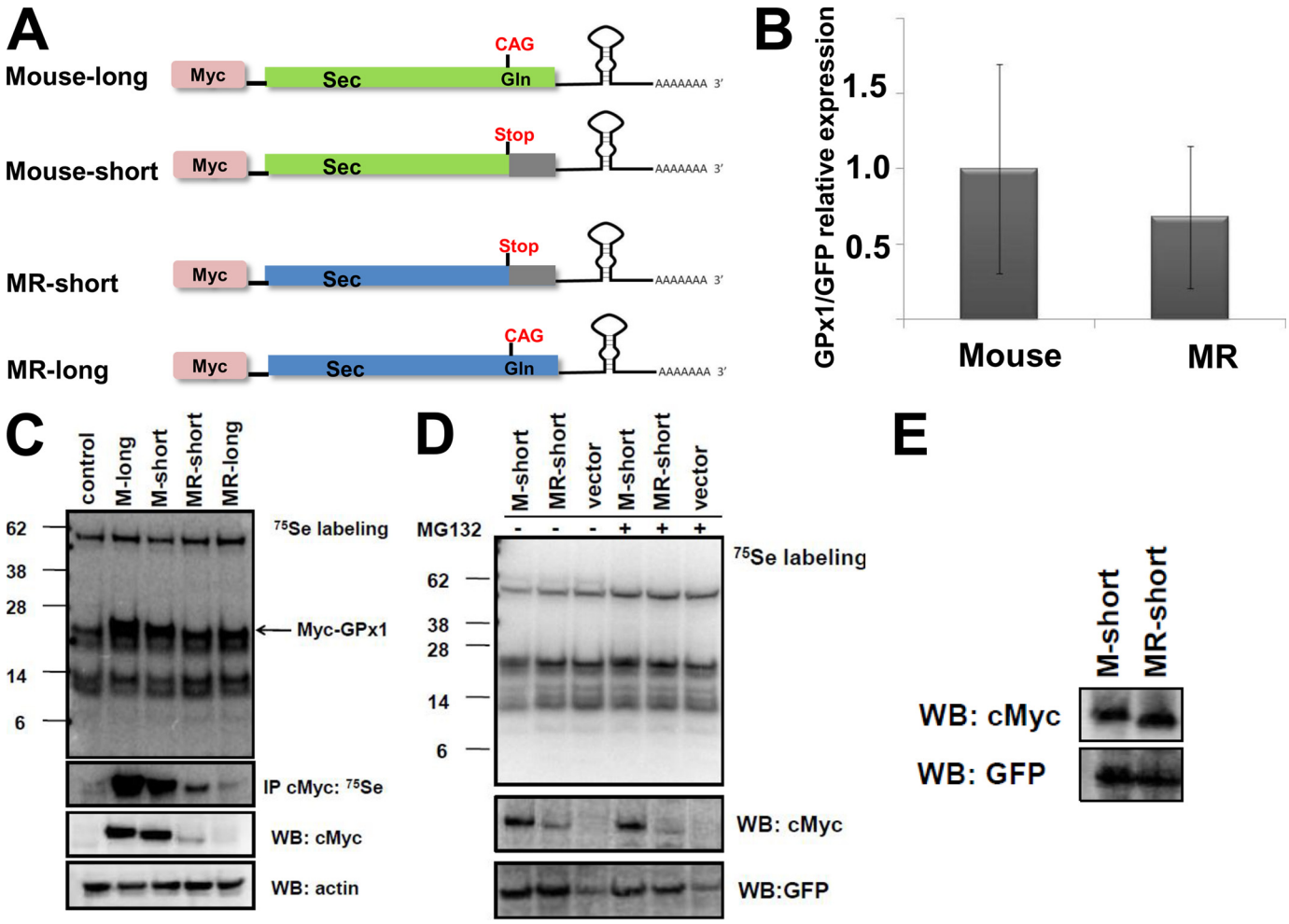


FIGURE 4. **GPx1 is poorly expressed in mammalian cells.** *A*, schematic representation of MR and mouse GPx1 mutant constructs. Positions of Sec and glutamine (CAG) codons, the stop signal (TAG), and the SECIS element in the 3′-UTR are shown. *B*, mRNA levels were assessed by real-time PCR and normalized to GFP expressed from the same vector. Results are given ± S.D. (*error bars*). *C*, MR and mouse Myc-GPx1 constructs were transfected into HEK 293 cells. Cells were labeled with $^{75}$Se, followed by SDS-PAGE and autoradiography (*top*). Migration of ectopically expressed GPx1 is shown on the *left*. The same lysates were probed with anti-Myc and anti-β-actin antibodies (*two bottom panels*). Myc-GPx1 mutants were also immunoprecipitated with anti-Myc antibodies, followed by PhosphorImager analysis of the $^{75}$Se-labeled GPx1. *D*, mouse and MR constructs were transfected into HEK 293 cells followed by treatment of cells with 10 μM MG132 for 12 h. Cells were labeled with $^{75}$Se, followed by protein analysis by SDS-PAGE and autoradiography (*top*). The same membrane was stained with Myc and GFP antibodies. *E*, expression of mouse and MR cysteine mutants of GPx1 in HEK 293 cells was analyzed by Western blotting. *IP*, immunoprecipitation; *WB*, Western blotting.

may be linked (*e.g.* inefficient Sec insertion may destabilize GPx1 mRNA).

*SECIS Element in MR GPx1 Is Not Responsible for Low GPx1 Expression*—Sec insertion includes recognition of the SECIS element in the 3′-UTR of selenoprotein mRNAs by SBP2 and subsequent recruitment of additional factors, such as EFSec and Sec-tRNA$^{[Ser]Sec}$, which insert Sec in response to the UGA codon. Efficiency of Sec incorporation may depend on additional features, such as the position of the UGA codon within the ORF and the type of SECIS element (32–34). Alignment of GPx1 SECIS elements revealed a nucleotide substitution in the conserved SBP2 binding site (Fig. 5*A*). However, comparison of MR (Fig. 5*B*) and mouse (Fig. 5*C*) SECIS elements in GPx1 did not show unusual features in the MR SECIS element, suggesting that the predicted structure may support Sec incorporation.

To directly test if the MR GPx1 SECIS element is responsible for the low GPx1 expression, we cloned coding sequences of mouse and MR GPx1s into pSelExpress1 vector containing a highly efficient eukaryotic SECIS element (27). Analysis of these expression constructs (containing the same SECIS element) by metabolic $^{75}$Se labeling of transfected HEK 293 cells showed that the MR GPx1 was still expressed at a low level compared with mouse GPx1 (Fig. 5*D*). To further examine the role of SECIS elements as well as the entire 3′-UTRs in GPx1 expression, we prepared constructs that swapped the 3′-UTRs between mouse and MR GPx1s. These constructs were expressed in HEK 293 cells, followed by $^{75}$Se labeling and Western blot analysis (Fig. 5*E*). Substitution of the MR GPx1 3′-UTR with that of the mouse did not increase MR GPx1 expression; in addition, replacement of the mouse GPx1 3′-UTR with that of the MR did not decrease the expression of mouse GPx1. Thus, neither the SECIS element nor the 3′-UTR were responsible for the reduced MR GPx1 expression. It is an attractive possibility that the overall GPx1 mRNA structure modulates the rate of Sec incorporation.

*Absence of GPx1 Decreases Selenium Levels in Mice*—GPx1 is the most abundant selenoprotein in mouse liver and kidney. We tested if removal of this protein could affect selenium levels

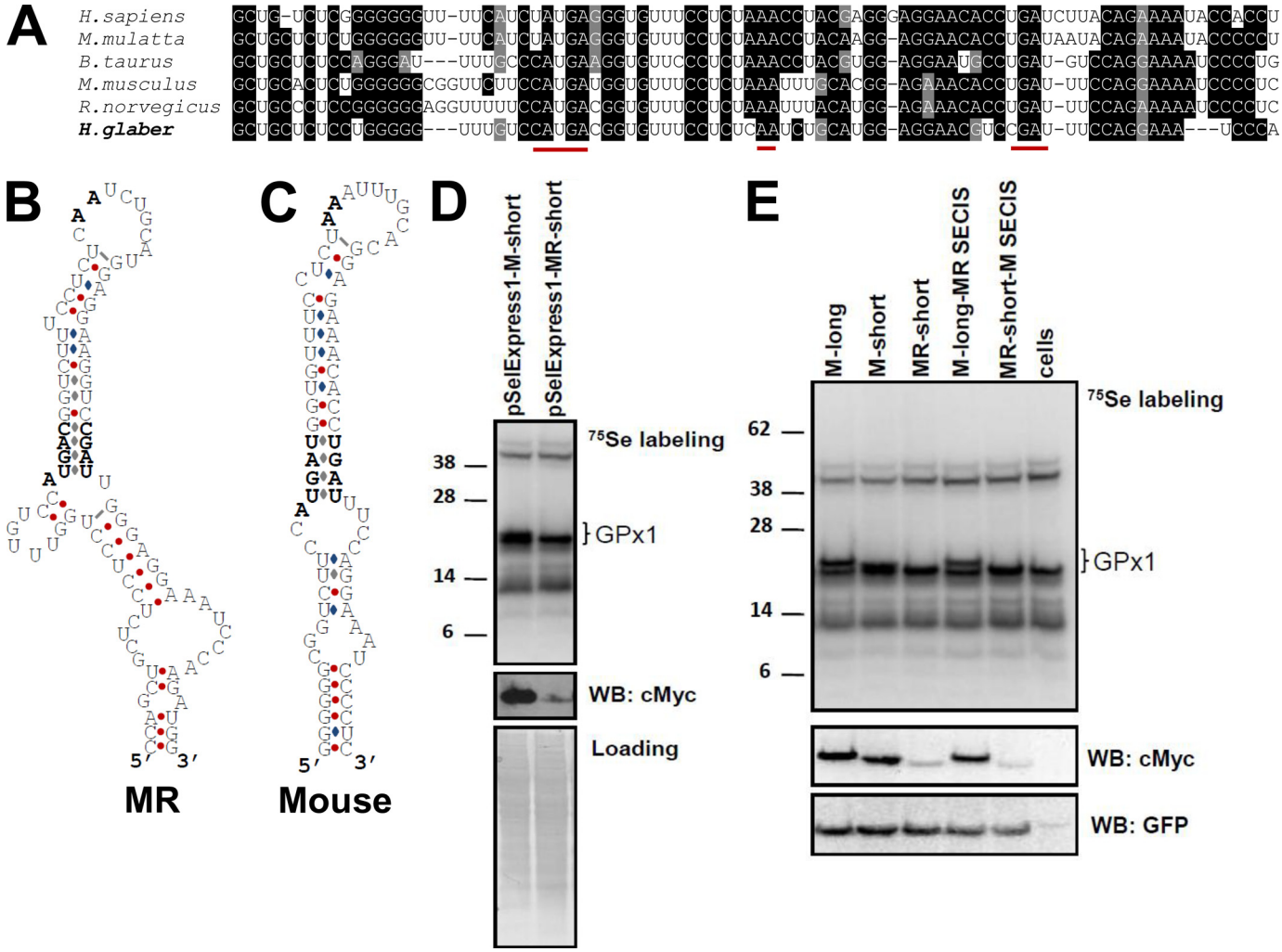


FIGURE 5. **SECIS element does not decrease GPx1 expression level.** *A*, alignment of mammalian GPx1 SECIS elements. Nucleotides critical for the SECIS function are *underlined*. *B*, MR GPx1 SECIS element as predicted by SECISearch. Functional sites are shown in *boldface type* (24). *C*, mouse GPx1 SECIS element. Functional sites are shown in *boldface type*. *D*, mouse and MR GPx1 coding sequences were cloned into pSelExpress1 containing an efficient eukaryotic SECIS element and expressed in HEK 293 cells. Cells were labeled with $^{75}$Se, followed by SDS-PAGE, autoradiography, and Western blotting with Myc antibodies. Coomassie staining is a loading control. *E*, coding sequences of mouse GPx1 containing the MR GPx1 3′-UTR (*M-long-MR SECIS*) and coding sequence of MR GPx1 containing mouse GPx1 3′-UTR (*MR-short-M SECIS*) were expressed in HEK 293 cells. Cells were labeled with $^{75}$Se, followed by SDS-PAGE, autoradiography, and Western blotting with Myc and GFP antibodies. *WB*, Western blot.

in tissues by examining WT and GPx1 knock-out mice. Selenium levels in GPx1 knock-out mice were almost twice as low as those in WT livers (Fig. 6) ($p$ = 0.00387) and kidneys ($p$ = 0.0409). However, in tissues characterized by lower GPx1 levels, such as spleen, heart, lung, and brain, selenium levels were not affected by GPx1 knock-out. Thus, the absence of GPx1 could indeed be responsible for the reduced selenium use by MRs.

*GPx1 Expression in Long Lived Rodents*—To examine if the aberrant expression of MR GPx1 has evolutionary aspects, we analyzed its levels in primary skin fibroblasts derived from long lived rodents, including white footed mouse, chipmunk, vole, single fox squirrel, beaver, and porcupine, and also examined fibroblasts from another long lived mammal, the little brown bat (35). Cells were metabolically labeled with $^{75}$Se, and proteins were analyzed by SDS-PAGE followed by autoradiography (supplemental Fig. S18*A*). HEK 293 cells were used as a positive control, and mouse embryonic fibroblasts were derived from GPx1 knock-out mice as a negative control. All analyzed species, except for the porcupine, had a strong band corresponding to GPx1. In the case of the porcupine, we observed a weak $^{75}$Se signal in the GPx1 position and a stronger band that migrated

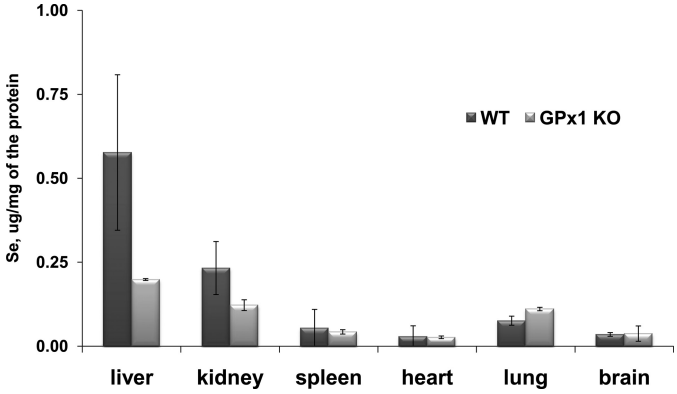


FIGURE 6. **Reduction in selenium levels in tissues of GPx1 KO mice.** Selenium was determined by ICP-MS in tissues from wild type (*WT*) and GPx1 knock-out (*KO*) mice. Values are means ± S.D. (*error bars*). Organs in which selenium was analyzed are shown *below* each *panel* (**, $p < 0.005$; *, $p < 0.05$).

faster than GPx1. Sequence analysis of GPx1 in these rodents should await the availability of their genome sequences. However, examination of the phylogenetic tree indicated that MR and porcupine share a common ancestor (supplemental Fig. S18*B*), whereas other examined mammals are more distant. Thus, it appears that the defect in GPx1 expression may not be limited to MR and may occur in a subset of rodents.

## DISCUSSION

GPx1 is an abundant glutathione peroxidase in mammals. It plays an important role in the protection of cells from oxidative stress by reducing hydrogen peroxide with glutathione. Surprisingly, we found that GPx1 is essentially absent in MR tissues, whereas other selenoproteins are expressed at normal levels and/or are enzymatically competent. Sequencing and analysis of the MR liver transcriptome detected GPx1 mRNA, but it was present at low levels and had an early termination codon. Further analyses revealed that the low expression was probably due to a combination of low mRNA levels and decreased insertion of Sec rather than due to compromised GPx1 activity caused by premature termination.

It was reported that GPx1 is the most abundant liver selenoprotein. In rat liver, it accounts for 63% of the total selenium (36). Selenium deficiency induces rapid degradation of GPx1 mRNA (and several other selenoprotein mRNAs), whereas the expression levels of several additional selenoproteins are preserved under these conditions (37). GPx1 was proposed as a biomarker of selenium utilization because its activity is very sensitive to selenium dietary status. It was also suggested that GPx1 is a "selenium buffer," wherein this enzyme stores selenium and provides this element for biosynthesis of selenoproteins during selenium deficiency (38). On the other hand, GPx1 knock-out does not affect expression of other selenoproteins (39, 40). This enzyme is also not essential. GPx1 knock-out animals are viable; however, they are more susceptible to oxidative stress and show defects in redox signaling (41). These data correlate with previously reported increases in oxidative stress parameters in MR, including a low GSH/GSSG ratio, high rate of DNA oxidative damage, and increased protein carbonylation and lipid peroxidation (10). Moreover, both GPx1 knock-out mice and MRs showed abnormal blood glucose regulation (39, 40). These mice had a normal fasting glucose but reduced blood insulin levels (41, 42). However, unlike GPx1 knock-out mice, MR also showed abnormal glucose tolerance (glucose levels remained elevated for prolonged periods of time) and insulin sensitivity (glucose levels immediately decreased upon insulin administration and remained low for prolonged periods of time) (10, 43). In addition, GPx1 knock-out mice had reduced islet $\beta$-cell mass in pancreatic tissue (42), whereas MR had different abundances of the four distinct types of islet cells. Although the abnormal glucose regulation may be relevant to MR adaptation to its specific lifestyle, it could be, at least in part, due to an abnormal GPx1 function.

Selenium levels in animal tissues vary depending on many factors, including the requirements of the organism for this trace element and the diet. Numerous studies have reported on the role of dietary selenium in human health. For example, selenium deficiency may cause endemic cardiomyopathy (Keshan disease), liver degeneration observed in rats and pigs, and white muscle disease in ruminants and turkeys (23, 44). None of the selenium deficiency-induced pathologies have been reported for MR. In this regard, it is particularly interesting that MRs have never been observed to develop cancer (2). We compared trace element profiles in control and GPx1 knock-out mice and found a significant decrease of tissue selenium levels in liver and kidney. Somewhat similar differences in selenium levels were observed between mouse and MR. GPx1 is the most abundant selenoprotein, especially in liver and kidney, and the GPx1 knock-out data suggest that this protein accounts for approximately half of selenium in these organs.

We also observed significant differences in selenium in spleen, lungs, and testes (these tissues depend on selenium provided by SelP). This selenoprotein is the only mammalian protein that contains multiple Sec residues (31). Previously, we suggested that the number of Sec residues in SelP might be used as an indirect genetic marker of selenium utilization (45). In rodents and primates, the Sec content of SelP is almost twice as low as in aquatic vertebrates. Comparison of rodent SelPs shows that *C. porcellus* and MR SelPs have 7 Sec residues, which is the lowest number of SelP Sec residues in vertebrates. MR, porcupine, and *C. porcellus* are closer to each other and are more distant from other rodents, such as mice, rats, and rabbits (46). Our analysis of GPx1 expression suggested a decreased GPx1 expression in MR and porcupine, and previous research revealed low GPx1 activity in *C. porcellus* (47). Overall, these data suggest a possible loss of GPx1 function in this specific group of rodents and, as a consequence, a reduced requirement for selenium by these organisms. It is remarkable that such an important selenoprotein is compromised in these animals, which survived for tens of millions of years essentially without GPx1.

*Acknowledgment—We thank Meenal Mhaskar for help with fibroblast cultures.*

## REFERENCES

1. Buffenstein, R. (2005) *J. Gerontol. A Biol. Sci. Med. Sci.* **60,** 1369–1377
2. Buffenstein, R. (2008) *J. Comp. Physiol. B* **178,** 439–445
3. Edrey, Y. H., Park, T. J., Kang, H., Biney, A., and Buffenstein, R. (2011) *Exp. Gerontol.* **46,** 116–123
4. McMullen, C. A., Andrade, F. H., and Crish, S. D. (2010) *Anat. Rec.* **293,** 918–923
5. Park, T. J., Lu, Y., Jüttner, R., Smith, E. S., Hu, J., Brand, A., Wetzel, C., Milenkovic, N., Erdmann, B., Heppenstall, P. A., Laurito, C. E., Wilson, S. P., and Lewin, G. R. (2008) *PLoS Biol.* **6,** e13
6. Woodley, R., and Buffenstein, R. (2002) *Comp. Biochem. Physiol. A Mol. Integr. Physiol.* **133,** 827–834
7. Larson, J., and Park, T. J. (2009) *Neuroreport* **20,** 1634–1637
8. Seluanov, A., Hine, C., Azpurua, J., Feigenson, M., Bozzella, M., Mao, Z., Catania, K. C., and Gorbunova, V. (2009) *Proc. Natl. Acad. Sci. U.S.A.* **106,** 19352–19357
9. Liang, S., Mele, J., Wu, Y., Buffenstein, R., and Hornsby, P. J. (2010) *Aging Cell* **9,** 626–635
10. Andziak, B., O'Connor, T. P., Qi, W., DeWaal, E. M., Pierce, A., Chaudhuri, A. R., Van Remmen, H., and Buffenstein, R. (2006) *Aging Cell* **5,** 463–471
11. Pérez, V. I., Buffenstein, R., Masamsetti, V., Leonard, S., Salmon, A. B., Mele, J., Andziak, B., Yang, T., Edrey, Y., Friguet, B., Ward, W., Richard-

son, A., and Chaudhuri, A. (2009) *Proc. Natl. Acad. Sci. U.S.A.* **106,** 3059–3064
12. Andziak, B., O'Connor, T. P., and Buffenstein, R. (2005) *Mech. Ageing Dev.* **126,** 1206–1212
13. Mills, G. C. (1957) *J. Biol. Chem.* **229,** 189–197
14. Lei, X. G., Cheng, W. H., and McClung, J. P. (2007) *Annu. Rev. Nutr.* **27,** 41–61
15. Lubos, E., Loscalzo, J., and Handy, D. E. (2010) *Antioxid. Redox Signal.*, in press
16. de Haan, J. B., Bladier, C., Griffiths, P., Kelner, M., O'Shea, R. D., Cheung, N. S., Bronson, R. T., Silvestro, M. J., Wild, S., Zheng, S. S., Beart, P. M., Hertzog, P. J., and Kola, I. (1998) *J. Biol. Chem.* **273,** 22528–22536
17. Fu, Y., Cheng, W. H., Porres, J. M., Ross, D. A., and Lei, X. G. (1999) *Free Radic. Biol. Med.* **27,** 605–611
18. Beck, M. A., Esworthy, R. S., Ho, Y. S., and Chu, F. F. (1998) *FASEB J.* **12,** 1143–1149
19. Gladyshev, V. N., Factor, V. M., Housseau, F., and Hatfield, D. L. (1998) *Biochem. Biophys. Res. Commun.* **251,** 488–493
20. Esworthy, R. S., Baker, M. A., and Chu, F. F. (1995) *Cancer Res.* **55,** 957–962
21. Moscow, J. A., Schmidt, L., Ingram, D. T., Gnarra, J., Johnson, B., and Cowan, K. H. (1994) *Carcinogenesis* **15,** 2769–2773
22. Ichimura, Y., Habuchi, T., Tsuchiya, N., Wang, L., Oyama, C., Sato, K., Nishiyama, H., Ogawa, O., and Kato, T. (2004) *J. Urol.* **172,** 728–732
23. Fairweather-Tait, S. J., Bao, Y., Broadley, M. R., Collings, R., Ford, D., Hesketh, J. E., and Hurst, R. (2011) *Antioxid. Redox Signal.* **14,** 1337–1383
24. Kryukov, G. V., Castellano, S., Novoselov, S. V., Lobanov, A. V., Zehtab, O., Guigó, R., and Gladyshev, V. N. (2003) *Science* **300,** 1439–1443
25. Twining, B. S., Baines, S. B., Fisher, N. S., Maser, J., Vogt, S., Jacobsen, C., Tovar-Sanchez, A., and Sañudo-Wilhelmy, S. A. (2003) *Anal. Chem.* **75,** 3806–3816
26. Lee, B. C., Le, D. T., and Gladyshev, V. N. (2008) *J. Biol. Chem.* **283,** 28361–28369
27. Novoselov, S. V., Lobanov, A. V., Hua, D., Kasaikina, M. V., Hatfield, D. L., and Gladyshev, V. N. (2007) *Proc. Natl. Acad. Sci. U.S.A.* **104,** 7857–7862
28. Kehr, S., Malinouski, M., Finney, L., Vogt, S., Labunskyy, V. M., Kasaikina, M. V., Carlson, B. A., Zhou, Y., Hatfield, D. L., and Gladyshev, V. N. (2009) *J. Mol. Biol.* **389,** 808–818
29. Schomburg, L., and Schweizer, U. (2009) *Biochim. Biophys. Acta* **1790,** 1453–1462
30. Lee, B. C., Dikiy, A., Kim, H. Y., and Gladyshev, V. N. (2009) *Biochim. Biophys. Acta* **1790,** 1471–1477
31. Burk, R. F., and Hill, K. E. (2009) *Biochim. Biophys. Acta* **1790,** 1441–1447
32. Donovan, J., and Copeland, P. R. (2010) *Antioxid. Redox Signal.* **12,** 881–892
33. Wen, W., Weiss, S. L., and Sunde, R. A. (1998) *J. Biol. Chem.* **273,** 28533–28541
34. Latrèche, L., Jean-Jean, O., Driscoll, D. M., and Chavatte, L. (2009) *Nucleic Acids Res.* **37,** 5868–5880
35. Leiser, S. F., and Miller, R. A. (2010) *Mol. Cell Biol.* **30,** 871–884
36. Behne, D., and Wolters, W. (1983) *J. Nutr.* **113,** 456–461
37. Sunde, R. A., Raines, A. M., Barnes, K. M., and Evenson, J. K. (2009) *Biosci. Rep.* **29,** 329–338
38. Sunde, R. A., Thompson, B. M., Palm, M. D., Weiss, S. L., Thompson, K. M., and Evenson, J. K. (1997) *Biomed. Environ. Sci.* **10,** 346–355
39. Lei, X. G. (2002) *Methods Enzymol.* **347,** 213–225
40. Lei, X. G., and Cheng, W. H. (2005) *J. Nutr.* **135,** 2295–2298
41. Lei, X. G., and Vatamaniuk, M. Z. (2011) *Antioxid. Redox Signal.* **14,** 489–503
42. Wang, X., Vatamaniuk, M. Z., Roneker, C. A., Pepper, M. P., Hu, L. G., Simmons, R. A., and Lei, X. G. (2011) *Antioxid. Redox Signal.* **14,** 391–401
43. Kramer, B., and Buffenstein, R. (2004) *Gen. Comp. Endocrinol.* **139,** 206–214
44. Mueller, A. S., Fischer, J., Most, E., and Pallauf, J. (2009) *J. Anim. Physiol. Anim. Nutr.* **93,** 313–324
45. Lobanov, A. V., Hatfield, D. L., and Gladyshev, V. N. (2008) *Genome Biol.* **9,** R62
46. Gorbunova, V., Bozzella, M. J., and Seluanov, A. (2008) *Age* **30,** 111–119
47. Jensen, C., and Pallauf, J. (2008) *J. Anim. Physiol. Anim. Nutr.* **92,** 481–491

**Supplementary Information**

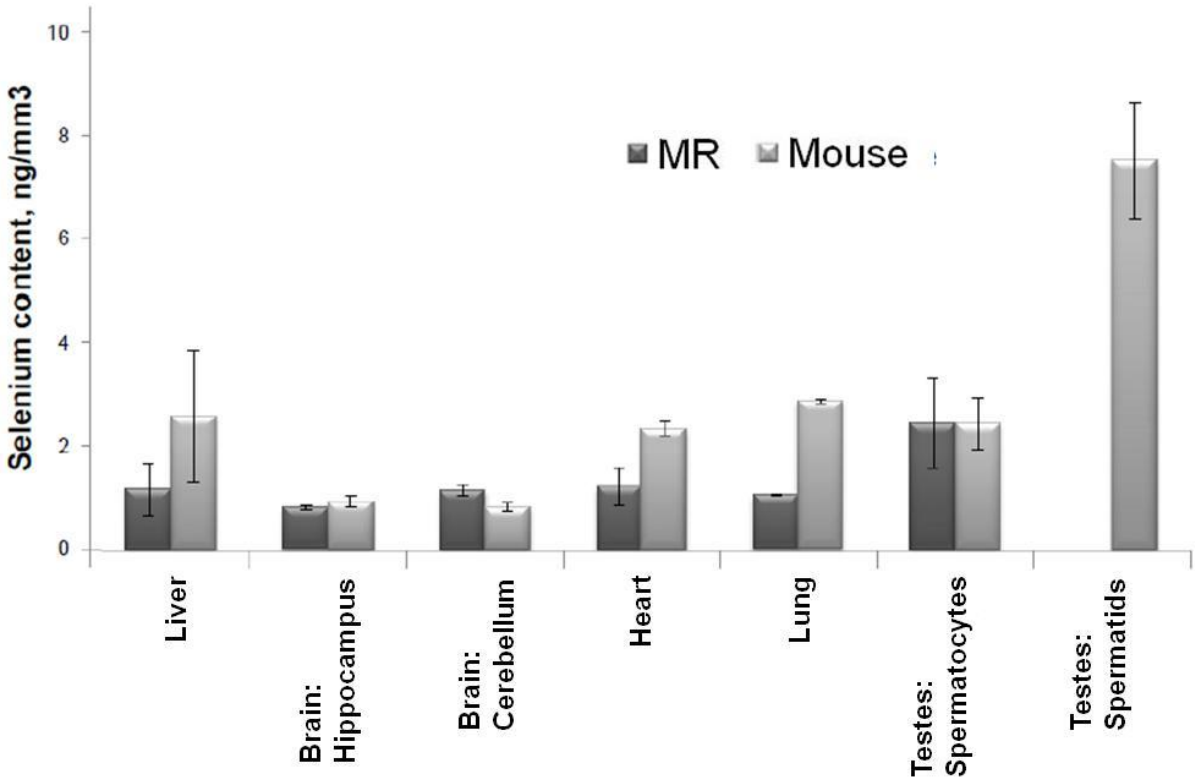


**Figure S1. Quantification of Se in mouse and MR tissues.** Se was quantified in XFM scans of similar areas of mouse and MR tissues. At least 3 representative XFM images were used for each quantification. Organs in which trace elements were analyzed are shown below each panel.

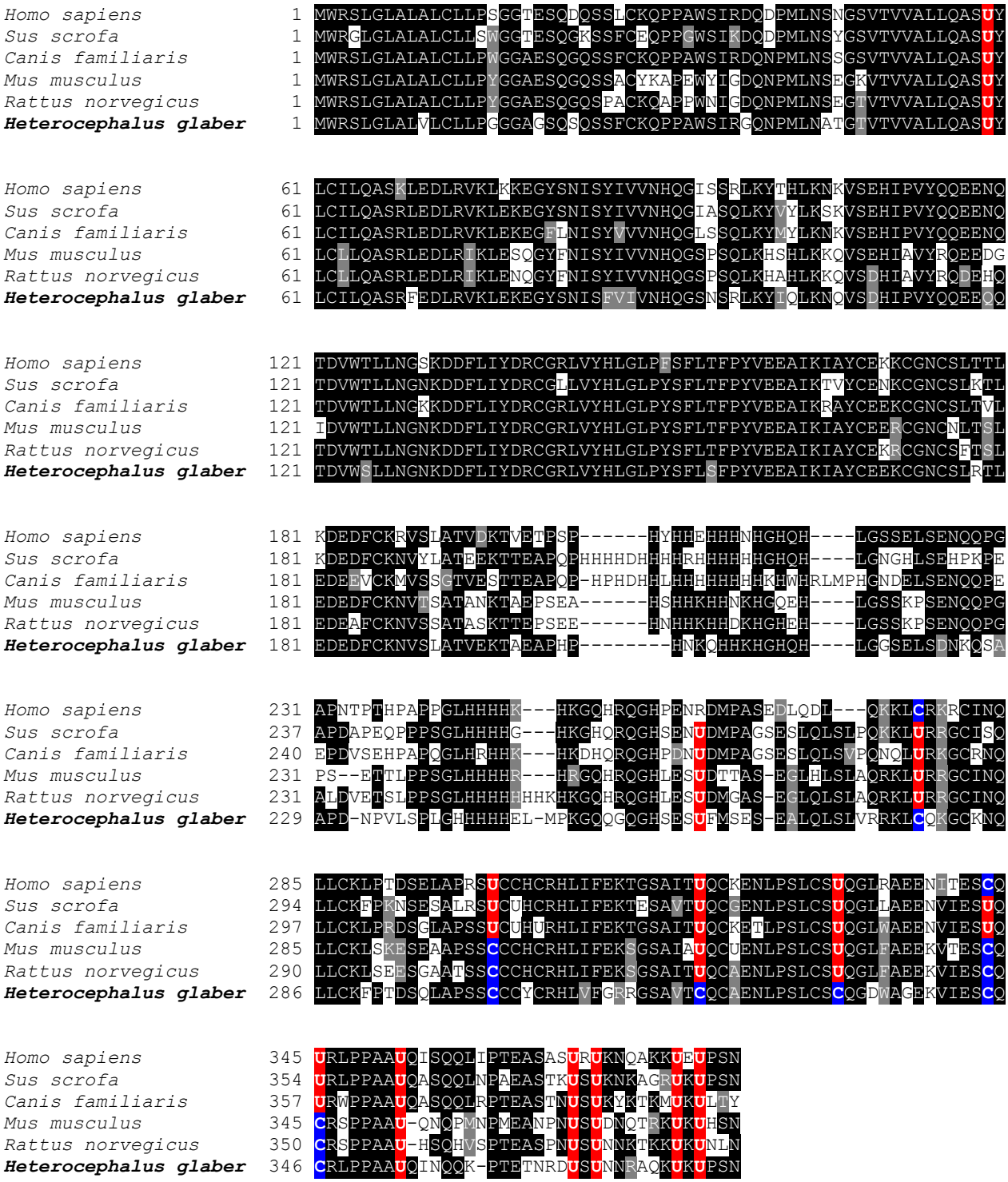


**Figure S2. Protein sequence alignment of SelP.** The following sequences were used for alignment construction (Genbank accession numbers): *Homo sapiens* (AAH58919.1); *Canis familiaris* (NP_001108590.1); *Sus scrofa* (NP_001128295.1); *Mus musculus* (AAH01991.2); and *Rattus norvegicus* (NP_062065.2). Selenocysteine residues are highlighted in red, and cysteines in the positions corresponding to selenocysteine are shown in blue.

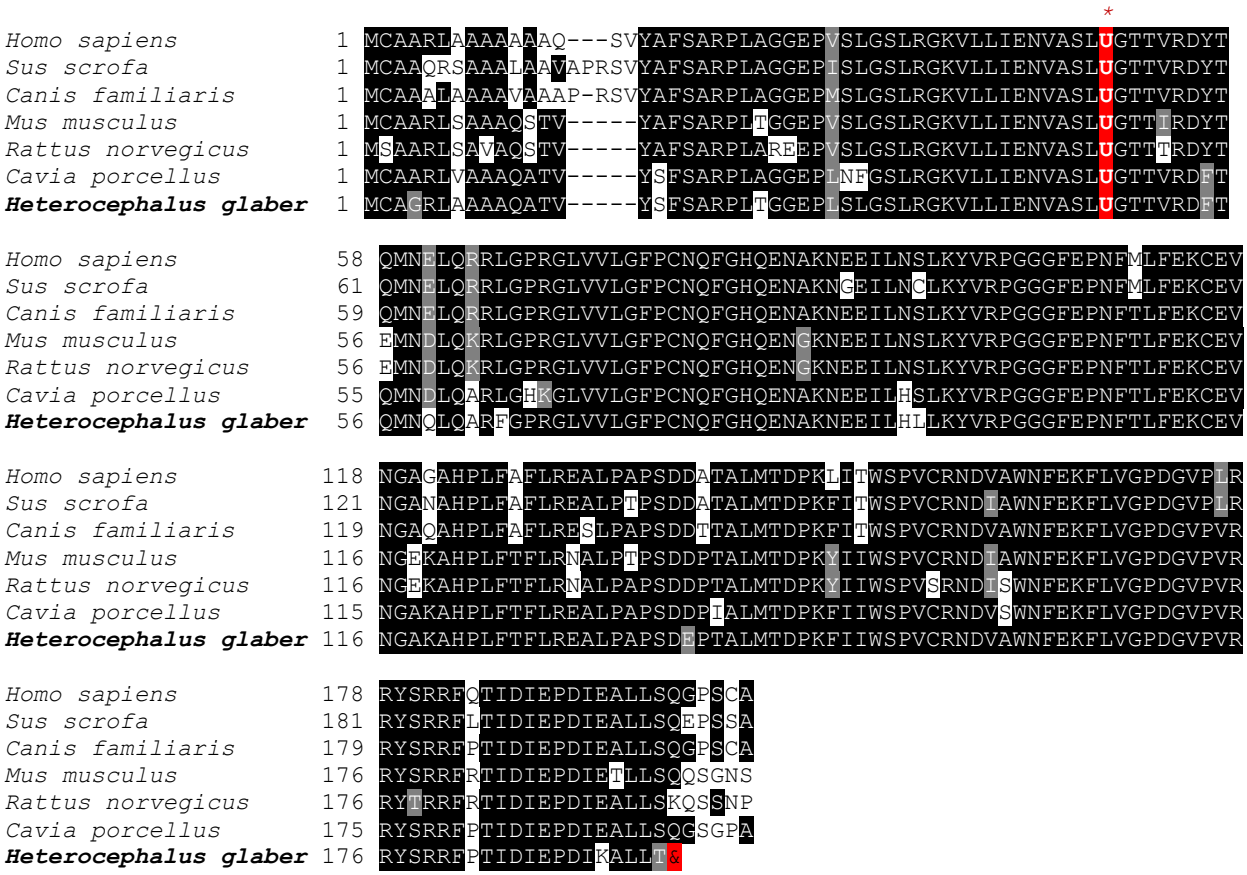


**Figure S3. Protein sequence alignment of GPx1.** The following sequences were used for alignment construction (Genbank accession numbers): *Homo sapiens* (NP_000572.2); *Sus scrofa* (NP_999366.1); *Canis familiaris* (NP_001108591); *Rattus norvegicus* (AAB95647.2), *Mus musculus* (CAA27558) and *Cavia porcellus* (AAKN02012894.1). The selenocysteine residue is highlighted in red and indicated by an asterisk. The early stop codon in the MR sequence is also highlighted in red.

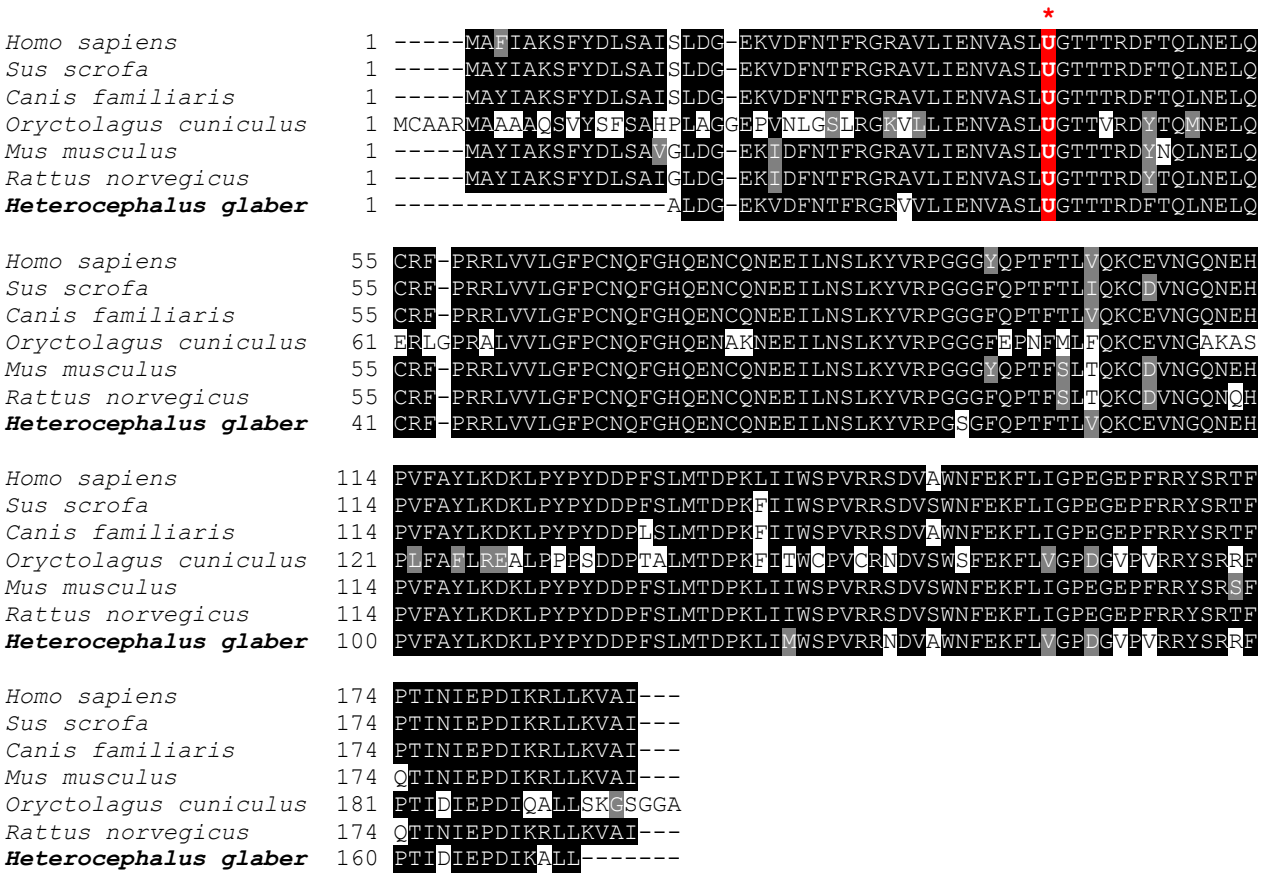


**Figure S4. Protein sequence alignment of GPx2.** The following sequences were used for alignment construction (Genbank accession numbers): *Homo sapiens* (NP_002074.2); *Sus scrofa* (NP_001108608.1); *Canis familiaris* (NP_001108607.1); *Oryctolagus cuniculus* (NP_001078913.1); *Rattus norvegicus* (NP_899653.2) and *Mus musculus* (NP_109602.2). The MR sequence is incomplete. The selenocysteine residue is highlighted in red and indicated by an asterisk.

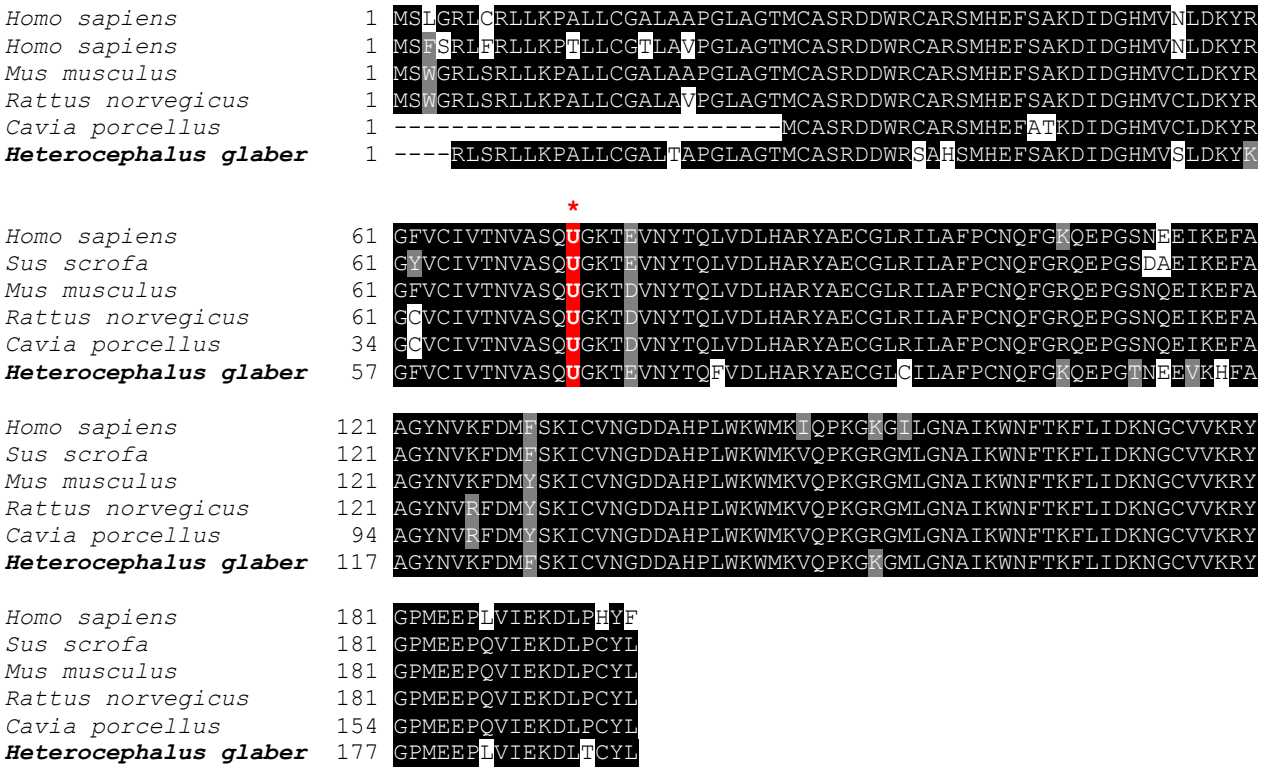


**Figure S5. Protein sequence alignment of GPx4.** The following sequences were used for alignment construction (Genbank accession numbers): *Homo sapiens* (NP_002076.2); *Sus scrofa* (NP_999572.1); *Mus musculus* (NP_032188.3); *Rattus norvegicus* (AAC52503.2); and *Cavia porcellus* (BAA92142.1). MR and *C. porcellus* sequences are incomplete. The selenocysteine residue is highlighted in red and indicated by an asterisk.


**Figure S6. Protein sequence alignment of SelW.** The following sequences were used for alignment construction (Genbank accession numbers): *Homo sapiens* (NP_003000.1); *Sus scrofa* (NP_999142.1); *Canis familiaris* (NP_001108484.1); *Mus musculus* (NP_033182.1); and *Rattus norvegicus* (NP_037159.3). The selenocysteine residue is highlighted in red and indicated by an asterisk.


**Figure S7. Protein sequence alignment of SelH.** The following sequences were used for alignment construction (Genbank accession numbers): *Homo sapiens* (NP_734467.1); *Sus scrofa* (NP_001171877.1); *Mus musculus* (NP_001028338.1); *Rattus norvegicus* (NP_001108411.1); and *Canis familiaris* (NP_001157978.1). The selenocysteine residue is highlighted in red and indicated by an asterisk.

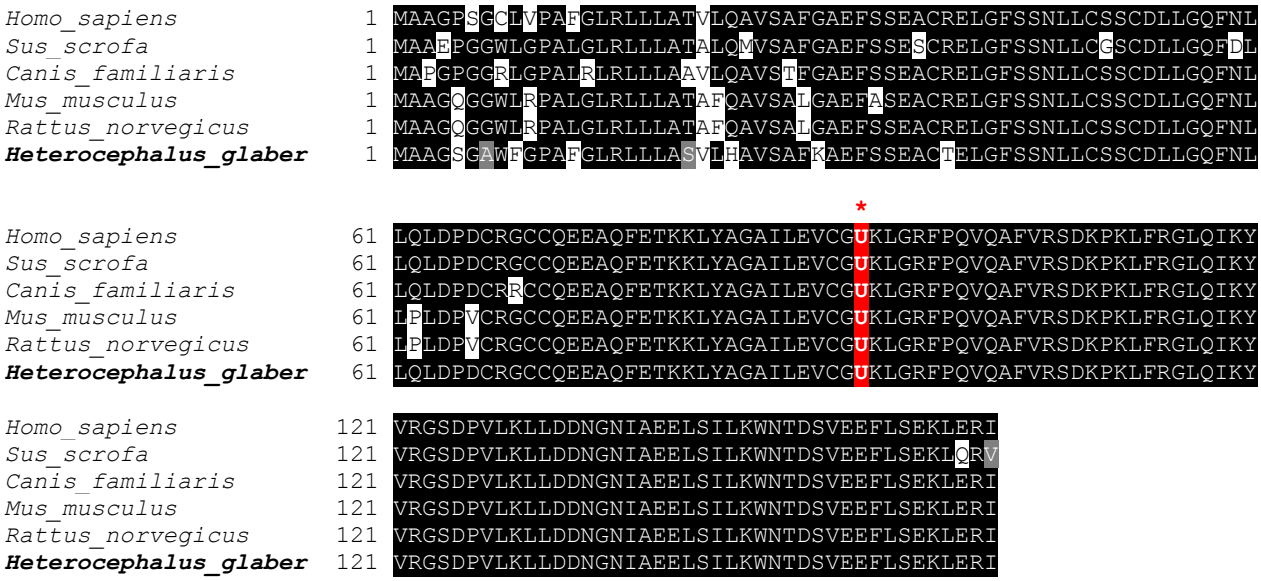


**Figure S8. Protein sequence alignment of the 15 kDa selenoprotein.** The following sequences were used for alignment construction (Genbank accession numbers): *Homo sapiens* (NP_004252.2); *Sus scrofa* (NP_001078912.1); *Rattus norvegicus* (NP_579831.2); *Mus musculus* (Q9ERR7.3); and *Canis familiaris* (NP_001108232.1). The selenocysteine residue is highlighted in red and indicated by an asterisk.

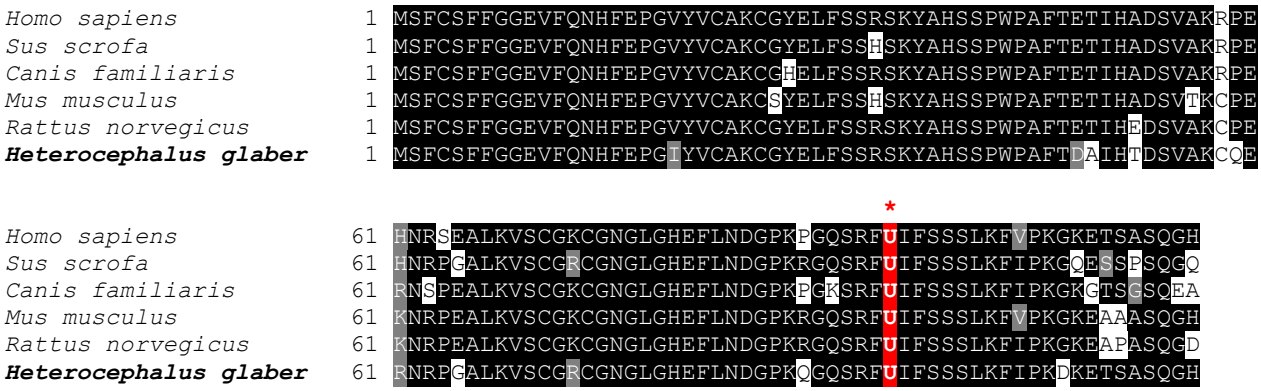


**Figure S9. Protein sequence alignment of MsrB1.** The following sequences were used for alignment construction (Genbank accession numbers): *Homo sapiens* (NP_057416.1); *Sus scrofa* (NP_001090929.1); *Canis familiaris* (NP_001108221.1); *Mus musculus* (AAI41147.1); and *Rattus norvegicus* (NP_001037750.2). The selenocysteine residue is highlighted in red and indicated by an asterisk.

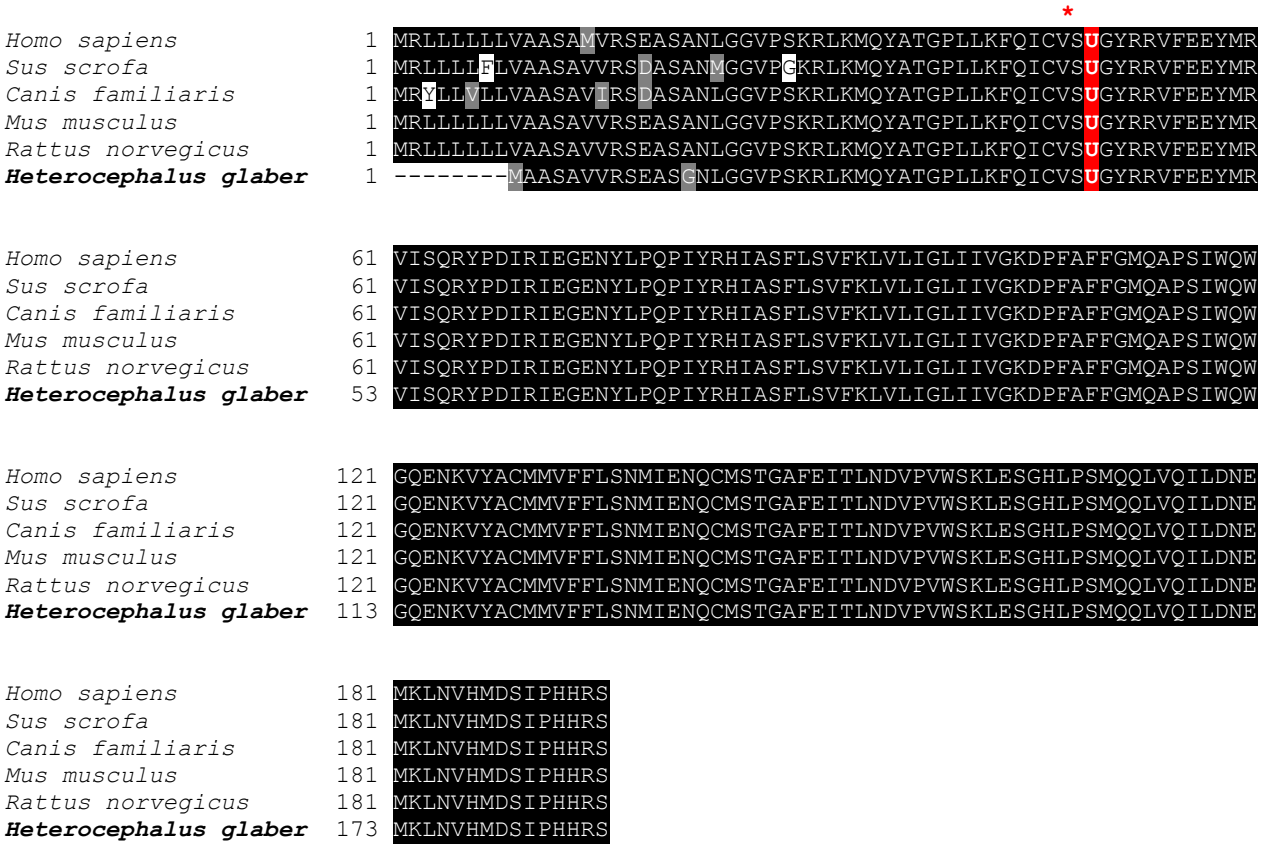


**Figure S10. Protein sequence alignment of SelT.** The following sequences were used for alignment construction (Genbank accession numbers): *Homo sapiens* (NP_057359.2); *Sus scrofa* (NP_001156880.1); *Canis familiaris* (NP_001157959.1); *Mus musculus* (NP_001035486.2); and *Rattus norvegicus* (NP_001014275.2). The selenocysteine residue is highlighted in red and indicated by an asterisk.

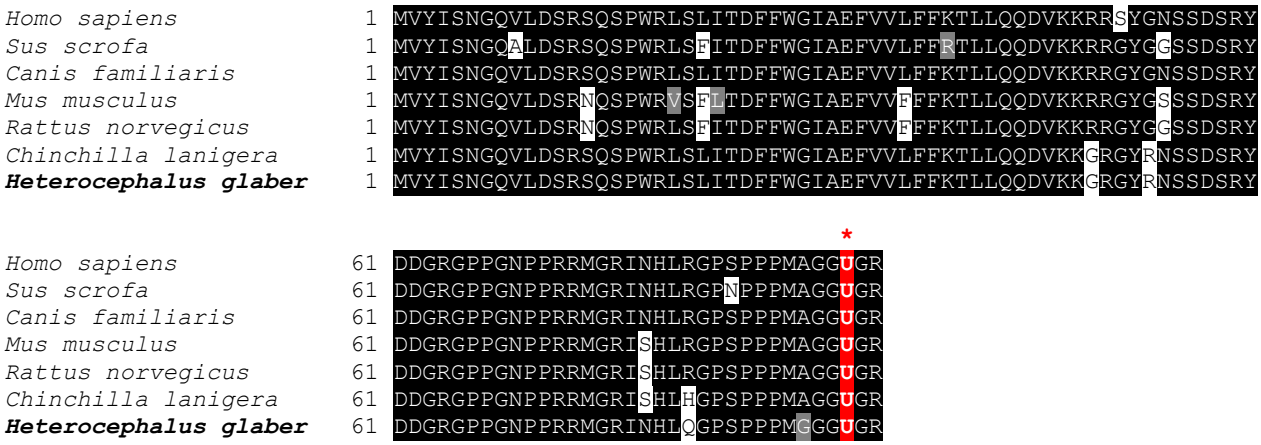


**Figure S11. Protein sequence alignment of SelK.** The following sequences were used for alignment construction (Genbank accession numbers): *Homo sapiens* (NP_067060.2); *Sus scrofa* (NP_001038018.2); *Canis familiaris* (NP_001108350.1); *Mus musculus* (NP_064363.2); *Rattus norvegicus* (NP_997472.2); and *Chinchilla lanigera* (AAR26540.1). The selenocysteine residue is highlighted in red and indicated by an asterisk.

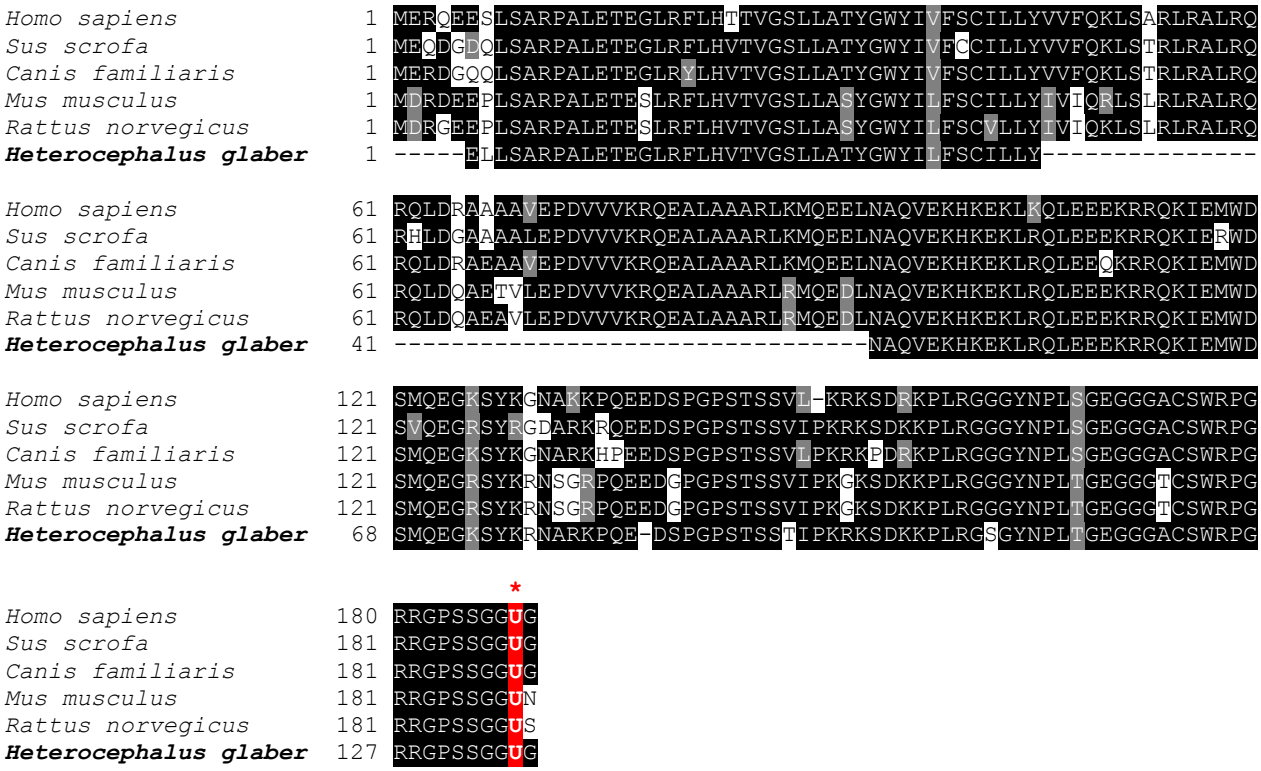


**Figure S12. Protein sequence alignment of SelS.** The following sequences were used for alignment construction (Genbank accession numbers): *Canis familiaris* (NP_001108229.1); *Homo sapiens* (NP_060915.2); *Mus musculus* (NP_077759.3); *Rattus norvegicus* (NP_775143.2); and *Sus scrofa* (NP_001157585.1). The MR sequence is incomplete. The selenocysteine residue is highlighted in red and indicated by an asterisk.

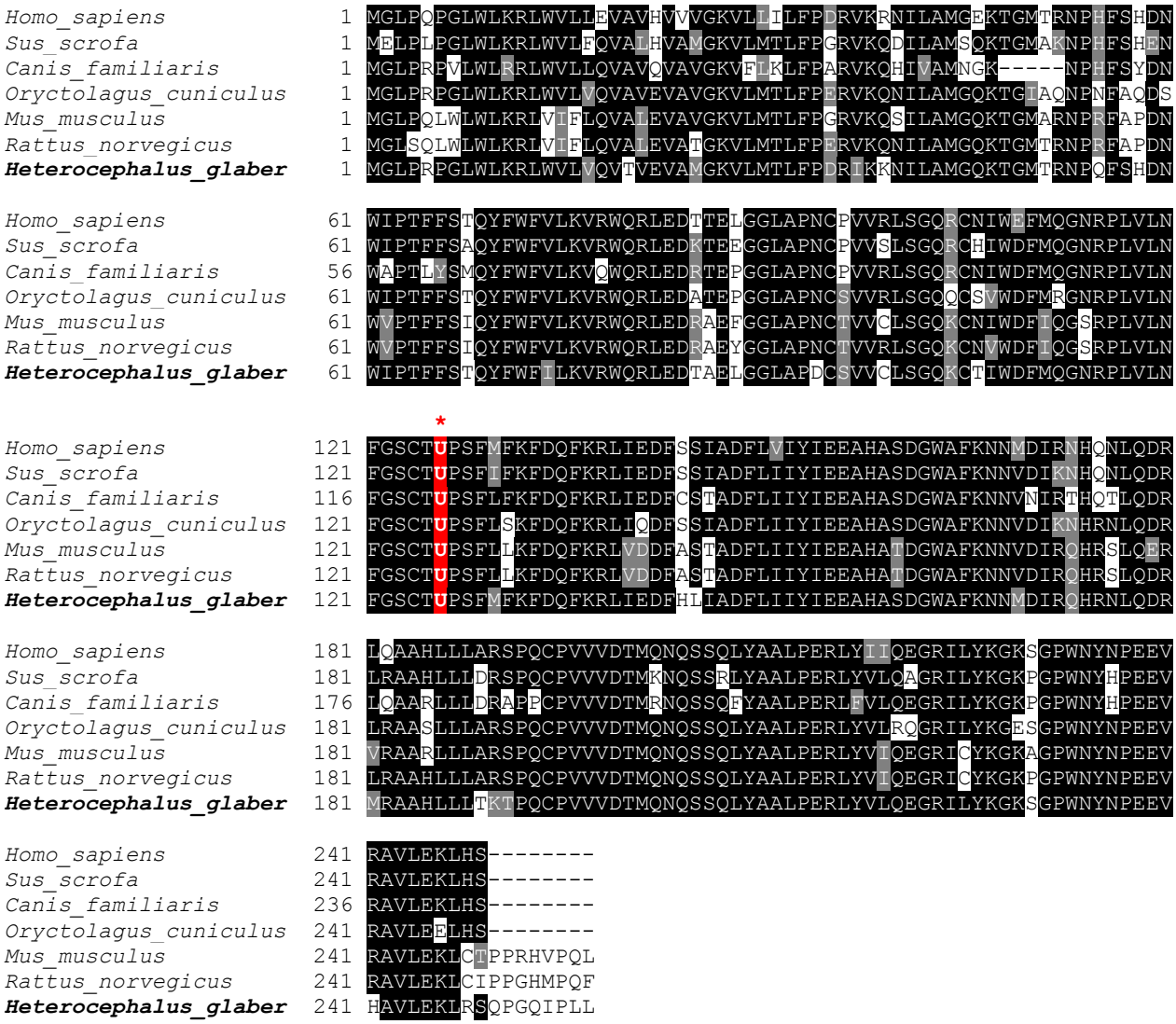


**Figure S13. Protein sequence alignment of DI1.** The following sequences were used for alignment construction (Genbank accession numbers): *Oryctolagus cuniculus* (NP_001093428.1); *Homo sapiens* (NP_000783.2); *Sus scrofa* (NP_001001627.1); *Mus musculus* (Q61153.3); *Rattus norvegicus* (NP_067685.5); and *Canis familiaris* (NP_001007127.1). The selenocysteine residue is highlighted in red and indicated by an asterisk.

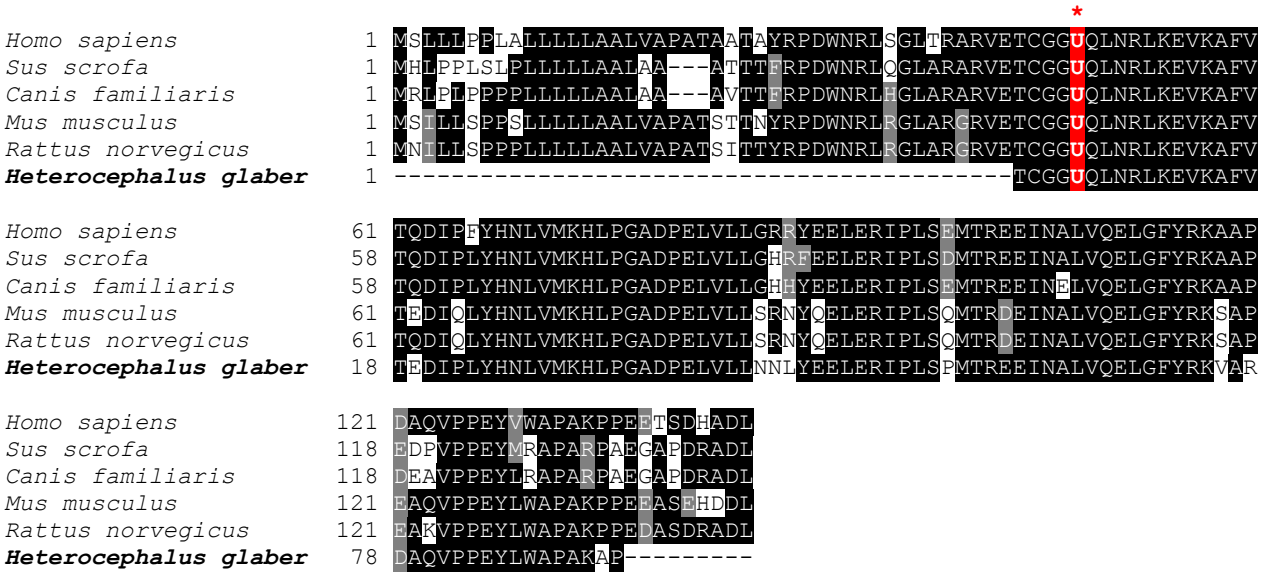


**Figure S14. Protein sequence alignment of SelM.** The following sequences were used for alignment construction (Genbank accession numbers): *Homo sapiens* (NP_536355.1); *Mus musculus* (NP_444497.1); *Rattus norvegicus* (NP_001108485.1); *Canis familiaris* (NP_001108486.1); and *Sus scrofa* (NP_001155120.1). The MR sequence is incomplete. The selenocysteine residue is highlighted in red and indicated by an asterisk.

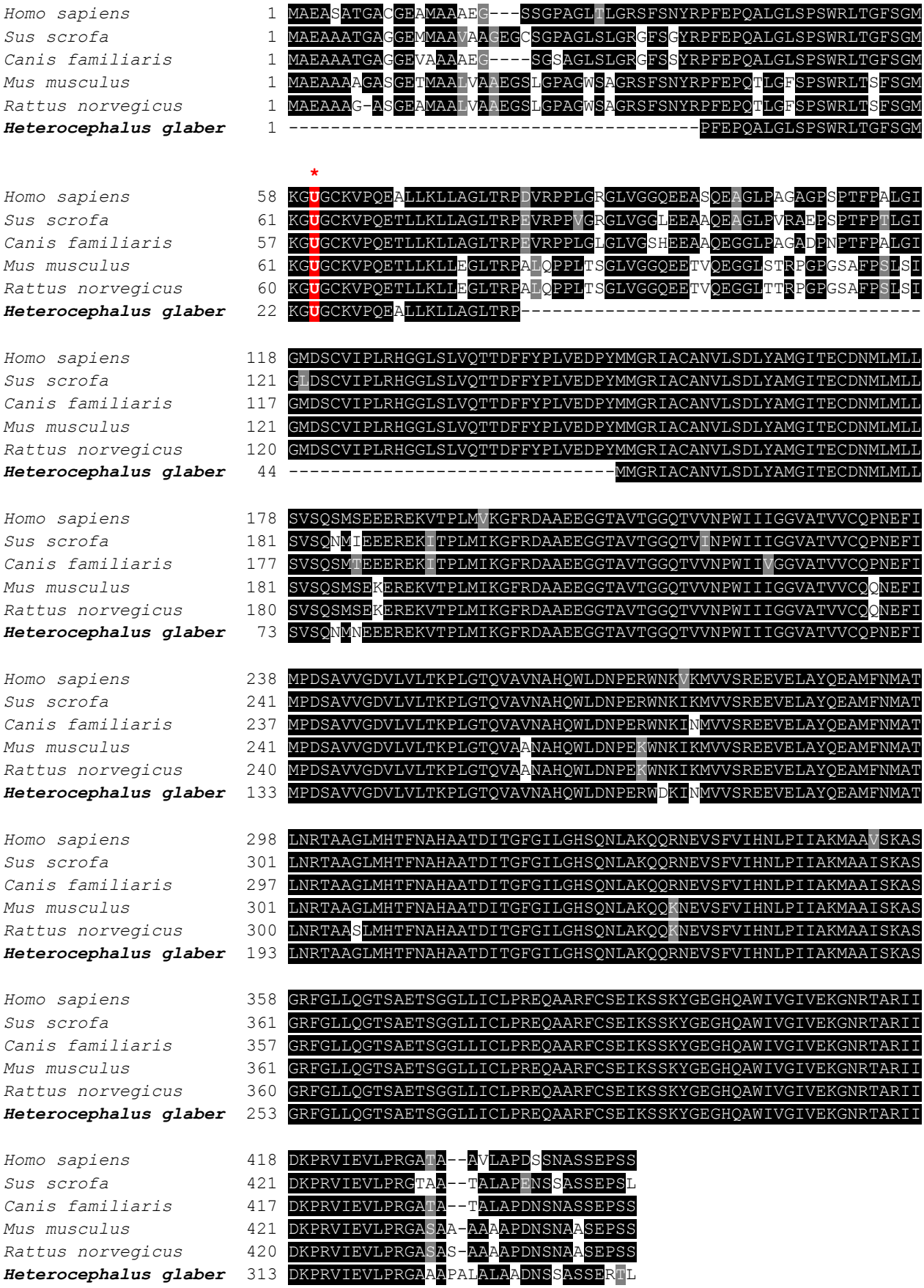


**Figure S15. Protein sequence alignment of SPS2.** The following sequences were used for alignment construction (Genbank accession numbers): *Canis familiaris* (NP_001108208.1); *Homo sapiens* (NP_036380.2); *Sus scrofa* (NP_001087204.1); *Rattus norvegicus* (NP_001073358.2); and *Mus musculus*

(NP_033292.2). The naked mole rat sequence is incomplete. The selenocysteine residue is highlighted in red and indicated by an asterisk.

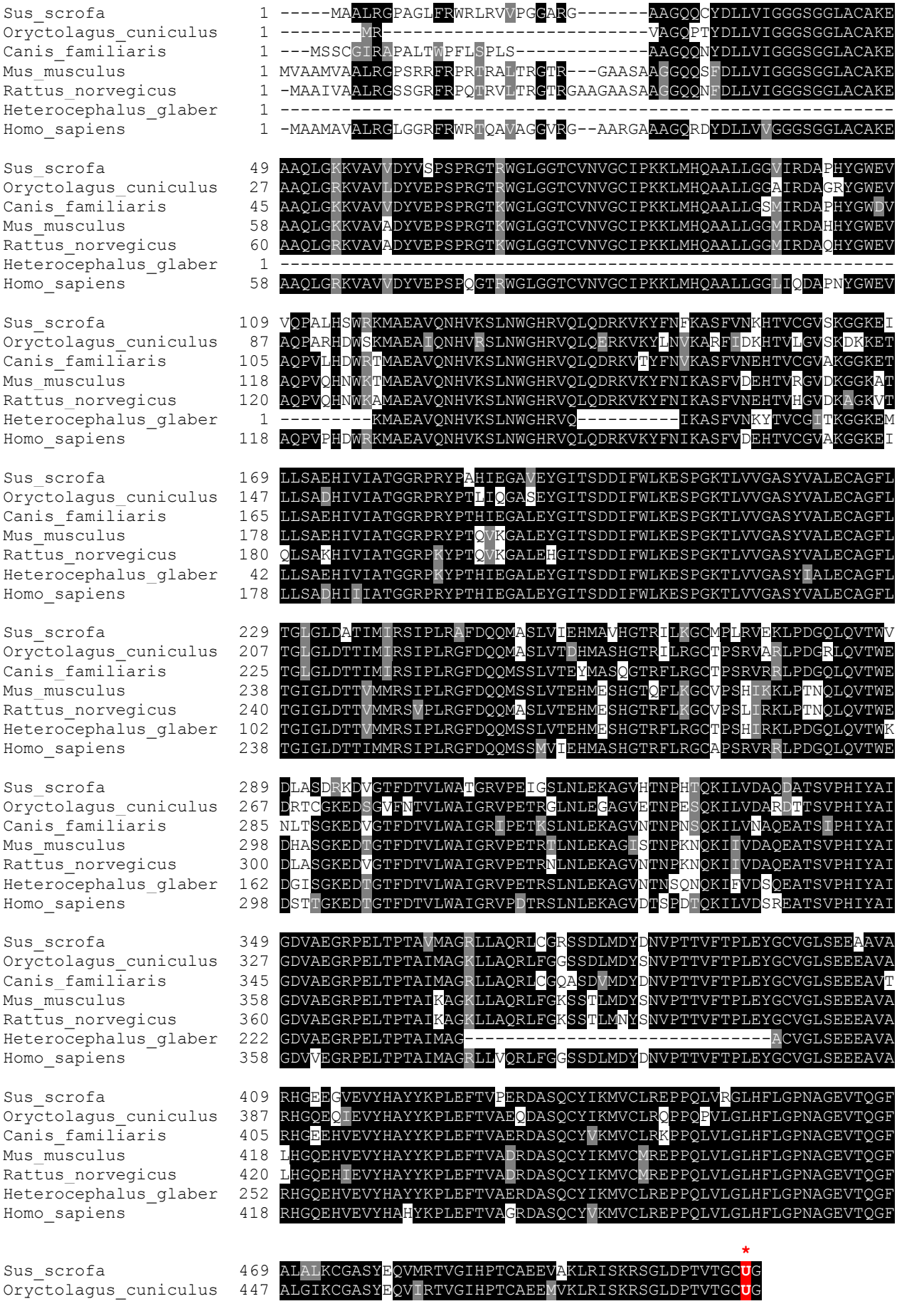

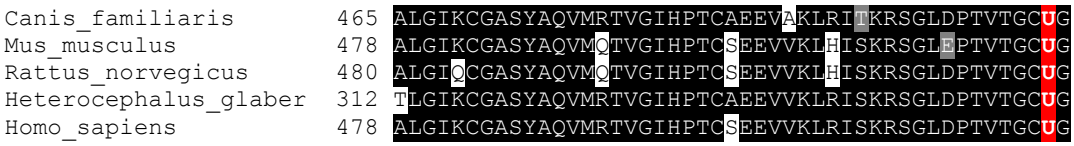


**Figure S16. Protein sequence alignment of mitochondrial thioredoxin reductase.** The following sequences were used for alignment construction (Genbank accession numbers): *Homo sapiens* (BAA77601.2); *Canis familiaris* (XP_850181.1); *Mus musculus* (Q9JLT4.4); *Rattus norvegicus* (NP_072106.1); *Sus scrofa* (NP_001162173.1); and *Oryctolagus cuniculus* (XP_002722800.1). The MR sequence is incomplete. The selenocysteine residue is highlighted in red and indicated by an asterisk.

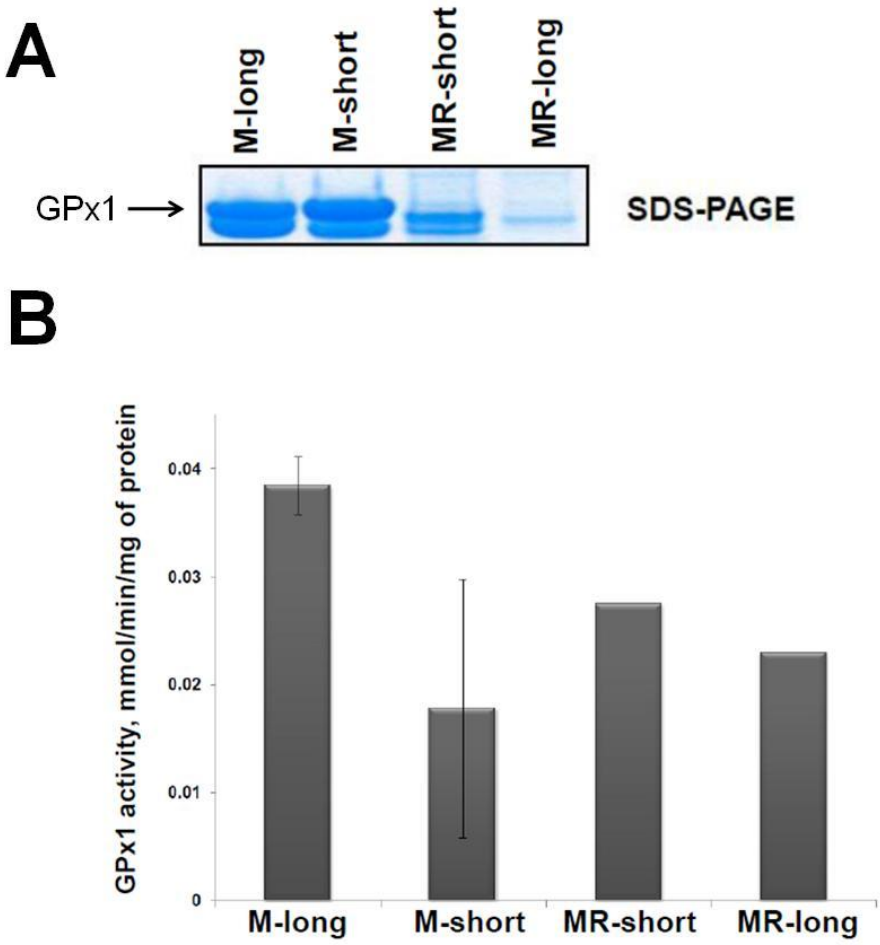


**Figure S17. Expression of mouse and MR GPx1 in *E. coli*.** Cysteine mutants of MR and mouse GPx1 were cloned into pET28a and expressed in *E. coli*. (A) Proteins were isolated from identical amounts of bacterial culture and aliquots were analyzed by SDS-PAGE. (B) Glutathione peroxidase activity of MR and mouse GPx1 was measured and normalized to the amount of protein in each sample. Results are given +/- SD.

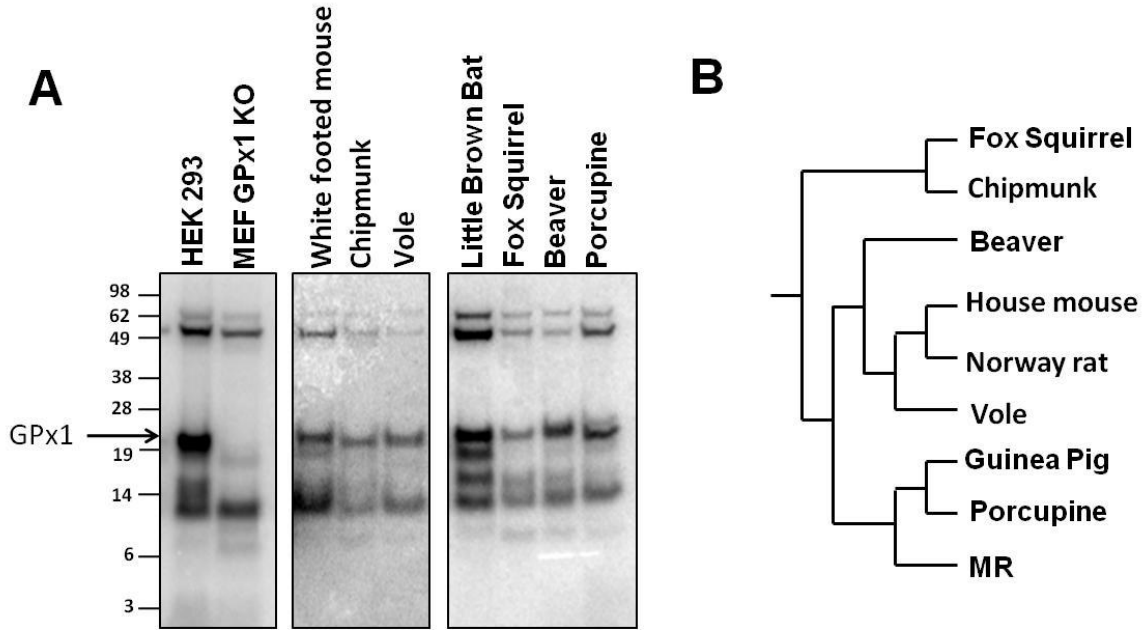


**Figure S18. Expression of GPx1 in skin fibroblasts of rodents and long lived mammals.** (A) Cells were labeled with $^{75}Se$ followed by SDS-PAGE and autoradiography. HEK 293 cells and MEFs derived from GPx1 KO mice were used as positive and negative controls, respectively. Migration of the band corresponding to GPx1 is shown with an arrow. (B) Schematic representation of the phylogenetic tree of rodents (adapted from (46)).